

PRELUDE TO A DOUBLE DEGENERATE MERGER: THE ONSET OF MASS TRANSFER AND ITS IMPACT ON GRAVITATIONAL WAVES AND SURFACE DETONATIONS

MARIUS DAN¹, STEPHAN ROSSWOG¹, JAMES GUILLOCHON², ENRICO RAMIREZ-RUIZ²

Draft version November 11, 2018

ABSTRACT

We present the results of a systematic numerical study of the onset of mass transfer in double degenerate binary systems and its impact on the subsequent evolution. All investigated systems belong to the regime of direct impact, unstable mass transfer. In all of the investigated cases, even those considered unstable by conventional stability analysis, we find a long-lived mass transfer phase continuing for as many as several dozen orbital periods. This settles a recent debate sparked by a discrepancy between earlier SPH calculations that showed disruptions after a few orbital periods and newer grid-based studies in which mass transfer continued for tens of orbits. The number of orbits a binary survives sensitively depends on the exact initial conditions. We find that the approximate initial conditions that have been used in most previous SPH calculations have a serious impact on all stages of the evolution from the onset of mass transfer up to the final structure of the remnant. We compare “approximate” initial conditions where spherical stars are placed at an initial separation obtained from an estimate of the Roche lobe size with “accurate” initial conditions that were constructed by carefully driving the binary system to equilibrium by a relaxation scheme. Simulations that use the approximate initial conditions underestimate the initial separation when mass transfer sets in, which yields a binary that only survives for only few orbits and thus a rapidly fading gravitational wave signal. Conversely, the accurate initial conditions produce a binary system in which the mass transfer phase is extended by almost two orders of magnitude in time, resulting in a gravitational wave signal with amplitude and frequency that remain essentially constant up until merger. The mass transfer also shows a unique oscillatory signal that is most pronounced for binary systems that are marginally unstable. As we show that these binaries can survive at small separation for hundreds of orbital periods, their associated gravitational wave signal should be included when calculating the gravitational wave foreground (although expected to be below LISA’s sensitivity at these high frequencies). We also show that the inclusion of the entropy increase associated with shock-heating of the accreted material reduces the number of orbits a binary survives given the same initial conditions, although the effect is not as pronounced when using the appropriate initial conditions. The use of accurate initial conditions and a correct treatment of shock heating allows for a reliable time evolution of the temperature, density, and angular momentum, which are important when considering thermonuclear events that may occur during the mass transfer phase and/or after merger. Our treatment allows us to accurately identify when surface detonations may occur in the lead-up to the merger, as well as the properties of final merger products.

Subject headings: supernova: general – WDs – nuclear reactions, nucleosynthesis, abundances – hydrodynamics

1. INTRODUCTION

White dwarfs (WDs) are the end point of the evolution of the vast majority of the stars in the universe. Our Galaxy harbours of order 10^{10} WDs (Napiwotzki 2009) and about 2.5×10^8 close binary WDs (Nelemans et al. 2001b), often referred to as double degenerates (DD). For about half of them a Hubble time is long enough so that gravitational wave emission can drive them to a phase of mass transfer. Such interacting DDs are suspected to produce observable objects such as sdB stars (Webbink 1984; Iben & Tutukov 1986; Saio & Jeffery 2000; Han et al. 2003), R Corona Borealis stars (Webbink 1984; Clayton et al. 2007), AM CVn stars (Paczynski 1967; Nelemans et al. 2001a; Solheim 2010) and, maybe most spectacularly, type Ia supernovae (Iben & Tutukov 1984; Webbink 1984). While for many years there was a strong inclination towards the single degenerate scenario, the recent discovery of “super-Chandrasekhar” events (Howell et al. 2006; Hicken et al. 2007; Yuan et al. 2007; Silverman et al. 2011) has re-strengthened the interest in DD mergers as possible type Ia progenitors. The lead-up to a merger includes a phase of mass transfer that is crucial for understanding the evolution and fates of double WD systems. This phase will affect the orbital evolution, the angular momentum and thermodynamical state of the final merger product, the associated gravitational wave signal, the environment into which any potential ejecta produced by an thermonuclear explosion will expand into, and whether or not a particular binary will merge at all. The numerical study of the onset of this mass transfer phase is the main topic of this investigation.

¹ School of Engineering and Science, Jacobs University Bremen, Campus Ring 1, 28759 Bremen, Germany; m.dan@jacobs-university.de, rosswog@jacobs-university.de

² TASC, Department of Astronomy and Astrophysics, University of California, Santa Cruz, CA 95064; jfg@ucolick.org, enrico@ucolick.org

The merger process of two WDs has been modeled by a number of groups (Benz et al. 1990; Rasio & Shapiro 1995; Segretain et al. 1997; Guerrero et al. 2004; Yoon et al. 2007; Pakmor et al. 2010), all of which use the smoothed particle hydrodynamics (SPH) method. In all of these simulations the mass transfer phase lasted for very few orbital time scales. Recently, grid-based simulations (Motl et al. 2002; D’Souza et al. 2006; Motl et al. 2007) were performed in which the authors carefully tried to reduce the angular momentum non-conservation due to advection errors that often plague grid-based codes (New & Tohline 1997). The latter results differed from the previous SPH calculations in that they showed long-lived mass transfer for many orbital periods and this has sparked some discussion about the stability of mass transfer in double degenerate systems during these late stages. Based on our experience in modeling the dynamics of neutron star black hole systems (Rosswog et al. 2004; Rosswog 2005), we had suspected that double WD binaries may be very sensitive to the exact initial conditions. As we will demonstrate below, the initial conditions used have a decisive impact and are one of the major reasons for the disagreement between various mass transfer calculations.

This is the companion paper of Guillochon et al. (2010), in which we focused on the fate of accreted helium in unstable, direct impact systems. The work showed that, contrary to prior belief, the mass transfer phase between two WDs may be eventful, and can be accompanied by Kelvin-Helmholtz-triggered thermonuclear surface explosions. These explosions may lead to the ignition of the accreting CO-WD in a double detonation scenario, which could be the long sought-after mechanism to initiate a type Ia supernova from WD binary merger. For the described work we had chosen a hybrid approach by combining results using the SPH method for the orbital evolution and the adaptive mesh refinement code FLASH (Fryxell et al. 2000) to focus on the evolution of the low-density helium material. We consider this a “best-of-both-worlds” approach, because it combines the major strengths of both Lagrangian and Eulerian methods. In this paper we present the details of the mass transfer/orbital evolution calculations that have been obtained with SPH, as well as a detailed comparison with the previously published FLASH calculations.

The main focus of this paper is the onset of the mass transfer and its impact on the orbital evolution; the structure of the resulting remnants will be discussed elsewhere. In Section 2 we briefly summarize conditions for the stability of mass transfer, in Section 3 we focus on the numerical aspects of the mass transfer modeling. We describe in detail how we construct our initial conditions and demonstrate their impact on the outcome of essentially every aspect of double degenerate merger simulations. We also briefly summarize the essential features of the SPH code that we are using. In a set of test calculations we explore to which extent the numerical resolution, the form of artificial viscosity, and the exact numerical initial conditions affect the results. In Section 4 we highlight results from two systems representative of a set of binary evolution calculations. In Sections 5 and 6 we discuss the implications of the extended mass transfer phase on the gravitational wave signal and the triggering of surface detonations prior to merger, respectively. We conclude the paper in Section 7 with a summary.

2. STABILITY OF MASS TRANSFER

In what follows we briefly collect the standard arguments on the stability of mass transfer (see e.g. Frank et al. 2002). Once stars are close enough that mass transfer via Roche lobe overflow can set in, the further evolution of the binary system depends on how both the orbit/Roche lobe size and the star react to the re-arrangement of mass and angular momentum. Due to their particular mass radius relation, WDs react to mass loss by expansion which tends to enhance the mass transfer rate. If mass is transferred to the heavier star, the orbit has to widen to ensure the conservation of the centre of mass and, therefore, mass transfer is tendentially quenched. The interplay of both effects determines the detailed orbital evolution. The total angular momentum of a point mass binary is given by

$$J = M_1 M_2 \left(\frac{Ga}{M_{\text{tot}}} \right)^{1/2}, \quad (1)$$

where the M_i are the masses, G is the gravitational constant, M_{tot} is the total mass and a the separation of the binary system. In the remainder of this work we will always denote the donor by label 2, the accretor by 1. On logarithmic differentiation one finds

$$\frac{\dot{a}}{2a} = \frac{\dot{J}}{J} - \frac{\dot{M}_2}{M_2} (1 - q), \quad (2)$$

where $q = M_2/M_1$. As expected, angular momentum loss tends ($\dot{J} < 0$) to shrink the orbit, while mass transfer ($\dot{M}_2 < 0$) tends to increase the orbital separation. The change of the donor Roche lobe size can be related to the change in orbital separation by logarithmically differentiating a simple Roche lobe size estimate (Paczynski 1971)

$$R_{L,2} = 0.462 a \left(\frac{q}{1+q} \right)^{1/3}, \quad (3)$$

which yields

$$\frac{\dot{R}_{L,2}}{R_{L,2}} = \frac{\dot{a}}{a} + \frac{1}{3} \frac{\dot{M}_2}{M_2}. \quad (4)$$

Using this to eliminate \dot{a} from Equation (2) then yields

$$\frac{\dot{R}_{L,2}}{R_{L,2}} = \frac{2\dot{J}}{J} + \frac{2\dot{M}_2}{M_2} \left(q - \frac{5}{6} \right), \quad (5)$$

and therefore for a mass ratio $q > 5/6$ a non-zero mass loss will trigger an expansion of the donor WD and at the same time shrink the Roche lobe size $R_{L,2}$. This will be further accelerated by any additional angular momentum loss, so with the used assumptions the mass transfer is clearly unstable in such cases.

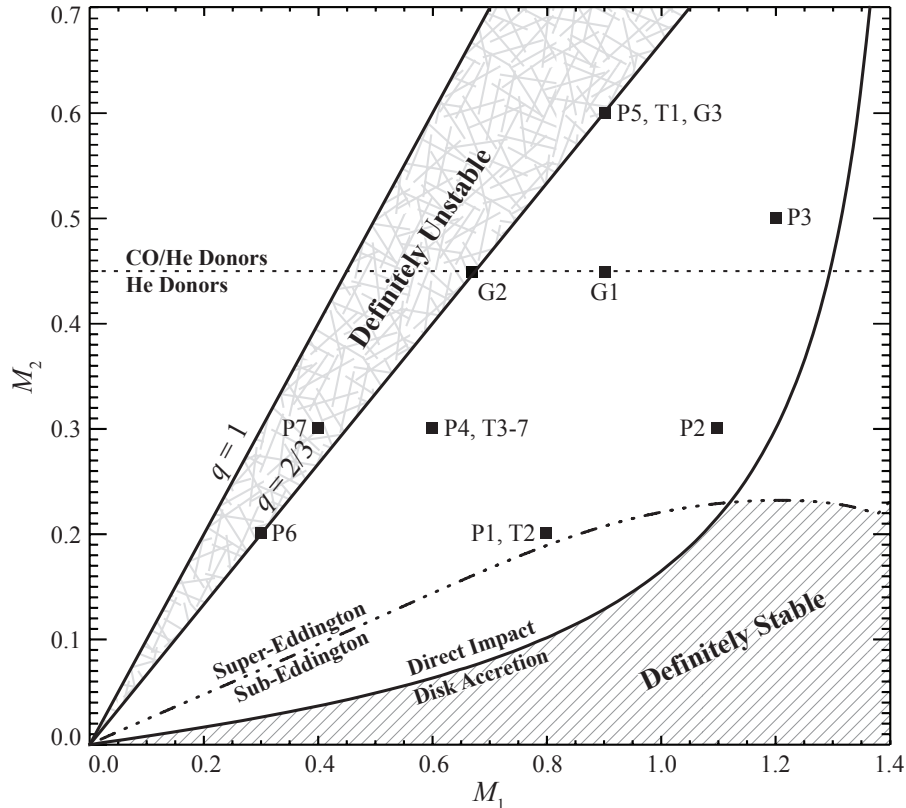


FIG. 1.— Analytical estimates of mass transfer stability in double WD binaries. The region below the lower solid line indicates the regime where a disk forms. Above the line, the accretion stream directly impacts on the accretor. The dot-dashed line separates systems that undergo sub- vs. super-Eddington accretion, with super-Eddington accretion possibly leading to an unstable binary. The hatched region of the plot indicates systems for which the accretion is both sub-Eddington and through a disk, which are almost certainly stable. For mass ratios q larger than $2/3$, the mass transfer is guaranteed to be unstable. The area between the regions of guaranteed stability and instability corresponds to the systems that can be either stable or unstable, depending on the spin-orbit coupling. The filled squares indicate the masses of the systems simulated in this work, see 1. Adapted from Marsh et al. (2004).

Of course, the so far discussed case is highly idealized. A point mass binary was assumed where the mass lost by the donor was completely incorporated into the accretor, while in reality mass can be lost from the system. Depending on whether or not the circularization radius exceeds the accretor radius, the transferred mass can either form a disk or it can impact directly onto the accretor surface. If a disk is formed, it would be tidally perturbed by the companion star and can thus feed back some fraction of the angular momentum into the orbit. In the direct impact case most of the angular momentum is invested into spinning up the accretor, which removes orbital angular momentum from and is therefore expected to destabilize the orbit. It should be noted, however, that a deformed donor can also feed back some angular momentum into the orbit. The orbit and the different binary components can exchange angular momentum both by advection of mass and by tides. Marsh et al. (2004) have generalized the simple treatment leading to Equation (2) for direct impact and tidal spin evolution

$$\frac{\dot{a}}{2a} = \frac{\dot{J}}{J_{\text{orb}}} - \left(\frac{\dot{J}_1 + \dot{J}_2}{J_{\text{orb}}} \right)_{\text{tid}} - \frac{\dot{M}_2}{M_2} \left[1 - q - \sqrt{(1+q)r_c} \right], \quad (6)$$

where r_c is the circularization radius in units of the orbital separation. The second term accounts for the exchange of angular momentum due to tides, the third term accounts for the spin of the accretor. If tides and accretor spin are ignored, Equation (6) reduces to (2). In Figure 1 we show the stability criteria for binaries of different donor and accretor masses, superimposed with the initial masses of our simulations (Table 1). Marsh et al. (2004) find the upper

left of the diagram to be guaranteed unstable, the lower right guaranteed stable and an uncertain region along the diagonal of the diagram. In this work we mainly investigate the “uncertain” region in the diagram.

3. NUMERICAL MODELING OF MASS TRANSFER

The main tool of this investigation is a 3D smoothed particle hydrodynamics (SPH) code. For recent reviews of the method see e.g. Monaghan (2005) and Rosswog (2009). The orbital dynamics of a binary system is very sensitive to the (re-)distribution of angular momentum and therefore a numerical simulation has to ensure very accurate angular momentum conservation. Its purely Lagrangian nature and the built-in conservation of mass, energy, linear and angular momentum (e.g. Section 2.4 in Rosswog 2009) make SPH a very powerful tool for this type of study. The conservation is exact up to effects that result from finite accuracy in gravitational forces due to the use of a tree, see below, and in the numerical integration of the ODE set. Both issues, however, are fully under control and can be improved to a desired level of accuracy by choosing the corresponding parameters for the tree and the ODE integration in an appropriate way, at the expense of a larger computational effort, though. For our parameters, even in the 84-orbit P1, corresponding to as many as 16,930 dynamical time scales of the $0.8 M_{\odot}$ star, energy and angular momentum are conserved to better than 1%. It has to be stated, however, that the advantage of *exact* mass conservation via constant SPH particle masses turns into a disadvantage if we are interested in the resolution of low-density portions of the flow. That is why we turned to the AMR code FLASH in Guillochon et al. (2010) to investigate the settling of the transferred material onto the accretor.

Details of our SPH code can be found in Rosswog et al. (2008). It uses an artificial viscosity scheme (Morris & Monaghan 1997) that reduces the dissipation terms to a very low level away from discontinuities, together with a switch (Balsara 1995) to suppress the spurious viscous forces in pure shear flows. The system of fluid equations is closed by the HELMHOLTZ equation of state (Timmes & Swesty 2000). It accepts an externally calculated nuclear composition and allows a convenient coupling to a nuclear reaction network. We use a minimal nuclear reaction network (Hix et al. 1998) to determine the evolution of the nuclear composition and to include the energetic feedback onto the gas from the nuclear reactions. A set of only seven abundance groups greatly reduces the computational burden, but still reproduces the energy generation of all burning stages from He burning to NSE accurately. We use a binary tree (Benz et al. 1990) to search for the neighbor particles and to calculate the gravitational forces.

Run No.	Masses [M_{\odot}]	Comp.	N_p [10^5]	$a_{0,9}$	P_0 [s]	$T_{\max,8}$	$\rho_{\max,7}$	L_{unb} [% L_{tot}]	M_{unb} [$10^{-3} M_{\odot}$]	N_{orb}	$a_{\text{dis},9}$	M_{trans} [M_{\odot}]	Comment
Production runs													
P1	0.2 + 0.8	He-CO	2	5.77	239	4.89	0.95	5.7	8.6	84	6.15	0.08	See 3.2.5, 4.1
P2	0.3 + 1.1	He-CO	2	4.75	151	12.23	6.15	7.11	17.6	59	5.01	0.13	
P3	0.5 + 1.2	He-ONeMg	2	3.35	81	18.85	15.44	4.86	17.4	31	3.27	0.09	
P4	0.3 + 0.6	He-CO	2	4.04	148	4.92	0.32	2.5	3.7	45	4.07	0.07	
P5 G3	0.6 + 0.9	CO-CO	2	2.68	62	10.6	1.75	0.8	1.85	29	2.58	0.10	See 3.2.5, 4.2 Guillochon et al.
P6	0.2 + 0.3	He-He	2	4.39	224	2.37	0.05	1.03	0.05	22	4.29	0.05	
P7	0.3 + 0.4	He-He	2	3.60	141	2.72	0.11	0.6	0.65	14	3.41	0.06	
P8	0.9 + 1.2	CO-CO	2	1.91	31	71.15	16.1	2.3	34.1	29	1.82	0.07	
Test runs													
G1	0.45 + 0.9	He-CO	1	3.36	91	16.11	1.59	2.2	4.6	30	3.35	0.12	Guillochon et al.
G2	0.45 + 0.67	He-CO	1	3.12	90	12.3	0.48	0.55	0.9	21	3.01	0.10	Guillochon et al.
T1	0.6 + 0.9	CO-CO	2	2.31	49	16.4	1.83	0.48	2.01	1	2.02	0.15	app. IC
T2	0.2 + 0.8	He-CO	2	4.95	190	5.24	0.96	1.91	1.8	2	4.43	0.08	app. IC
T3	0.3 + 0.6	He-CO	2	3.89	139	5.59	0.33	0.4	0.5	6	3.64	0.08	$a_0 = 1.13 a_0^{\text{EG}}$
T4	0.3 + 0.6	He-CO	0.4	4.00	145	4.99	0.35	2.1	2.6	20	4.0	0.07	AV_1
T5	0.3 + 0.6	He-CO	0.4	4.00	145	6.10	0.36	1.91	2.5	23	3.99	0.08	AV_2
T6	0.3 + 0.6	He-CO	0.4	4.00	145	4.70	0.33	2.09	2.6	18	4.00	0.08	AV_3
T7	0.3 + 0.6	He-CO	0.4	4.00	145	3.99	0.31	2.13	2.5	19	4.12	0.07	AV_4

TABLE 1

SUMMARY OF THE RUNS PERFORMED FOR THIS PAPER. $a_{0,9}$ IS THE INITIAL SEPARATION IN UNITS OF 10^9 CM, $T_{\max,8}$ IS THE PEAK TEMPERATURE IN UNITS OF 10^8 K, $\rho_{\max,7}$ THE PEAK DENSITY IN UNITS OF 10^7 G CM $^{-3}$ AND L_{unb} IS THE FRACTION OF ANGULAR MOMENTUM CONTAINED IN MATERIAL THAT IS UNBOUND AT THE END OF THE SIMULATION. $a_{\text{dis},9}$ IS THE SEPARATION (IN 10^9 CM) AT WHICH TIDAL DISRUPTION OF THE DONOR OCCURS AND M_{trans} IS THE AMOUNT OF MATERIAL (IN M_{\odot}) LOST BY THE DONOR PRIOR TO DISRUPTION.

3.1. Initial conditions

In what follows we will summarize how initial conditions are constructed for double WD binary systems, both in this and in previous work.

3.1.1. Previous work

In their pioneering work, Benz et al. (1990) followed the dynamical evolution of a $0.9 + 1.2 M_{\odot}$ WD binary system. They constructed cold, isolated WDs in hydrostatic equilibrium and placed them without spin-rotation at an initial

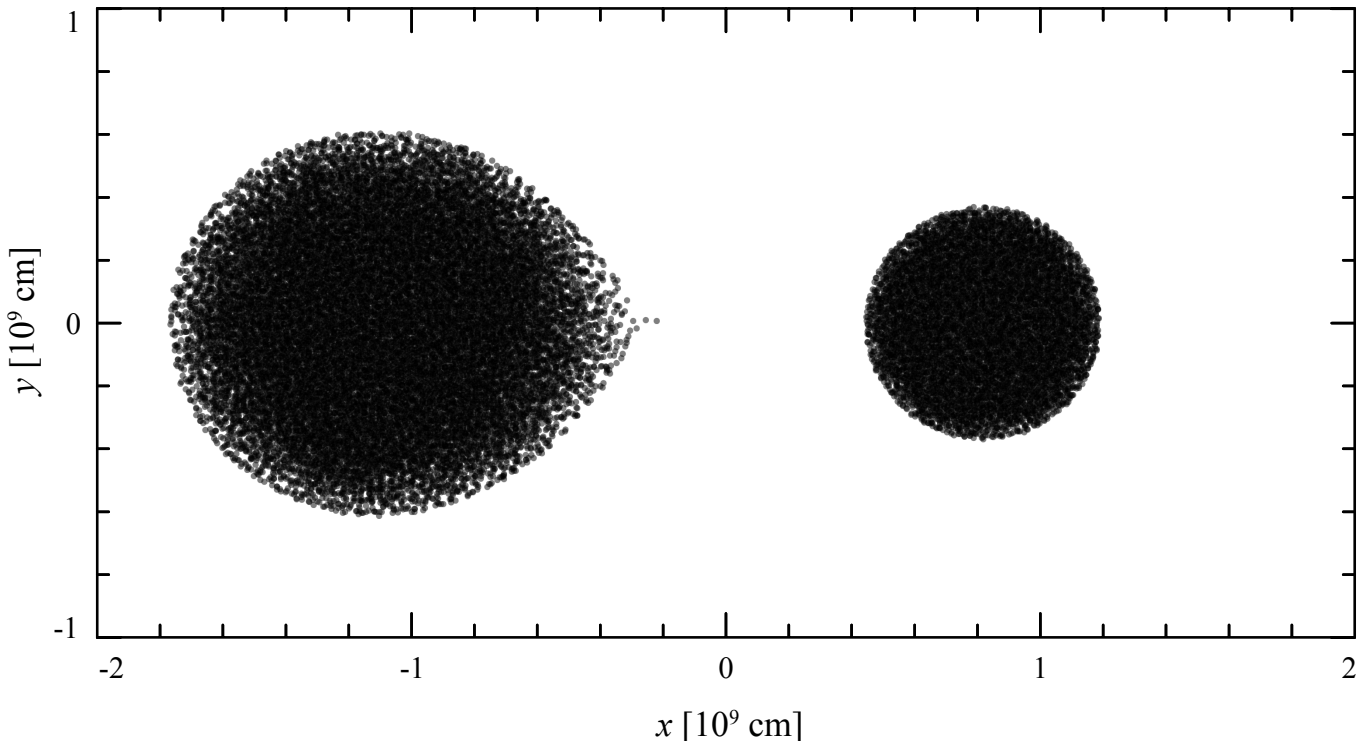


FIG. 2.— Equilibrium configuration ($0.9 + 1.2 M_{\odot}$) at the onset of mass transfer. The figure shows a projection of the SPH particles onto the orbital plane. Each particle’s location within this plane is shown as a translucent grey circle.

separation such that the secondary’s Roche radius was smaller than its unperturbed initial radius by 8%. One of the major conclusions of Benz et al. was that within about two orbital periods the secondary is completely destroyed and transformed into a thick accretion disk around the accretor. As we will show below, this short time to merger is an artifact of the initial separation being too small. We have followed the recipe of Benz et al. for the initial conditions and find exactly the same result as presented in their paper. We have further compared the orbital evolution of a 50,000 particle binary system, once according to the original Benz et al. description and according to our scheme, as described in Section 3.1.2. Again, with their initial conditions the merger set in within about one orbital period. With our initial conditions and everything else being the same, the binary survived for 14 orbits of continued mass transfer.

In Segretain et al. (1997) and Yoon et al. (2007) the stars were placed at a mutual separation so that the secondary fills its Roche lobe. In Segretain et al. the WDs had no initial spin, while in Yoon et al. the WDs begin tidally locked. Guerrero et al. (2004) and Lorén-Aguilar et al. (2009) initially placed the stars in a detached configuration and then slowly decreased the separation to the point where mass transfer began. However, their relaxation procedure did not allow the stars to reach complete hydrostatic equilibrium. If the stars are brought together too quickly, this can cause undesired (and unrealistic) oscillations in the WDs and may again lead to an abbreviated mass transfer phase. For example, the mass transfer phase in their $0.4 + 1.2 M_{\odot}$ system (Figure 10 in Guerrero et al. (2004)) only lasts for a single orbit. This is also the case for the simulation of a $0.6 + 0.8 M_{\odot}$ system (see Figures 1 and 2 in Lorén-Aguilar et al. 2009).

Our initial conditions are constructed in a way that is similar to Rasio & Shapiro (1995) (Section 3.1.2). Rasio & Shapiro constructed a synchronized binary system with mass ratio of $q = 0.5$, and also followed the dynamical evolution once a few particles had crossed the L_1 point. They found a merger after five orbital periods and also questioned the earlier use of non-equilibrium initial conditions. We have tried to reproduce their calculations as closely as possible by adopting the same particle number, equation of state, and the same prescription for evolving the entropic function $K(s)$ (Equation (12)), but still we only found a merger after fifteen orbital periods. Fryer & Diehl (2008) place the two stars close enough such that the donor is already overflowing its Roche radius, which leads to a premature merger. The recent work of Pakmor et al. (2010) focuses primarily on the coalescence of the binary, but their initial conditions are not appropriate for studies of long-term stability.

3.1.2. Our approach

We primarily focus on synchronized binary systems, but we also perform some tests with initially non-spinning WDs. Our procedure is similar to the one described in Rosswog et al. (2004). We begin our initialization procedure with stars that are set up according to one-dimensional, cold ($T = 10^5$ K) equilibrium models. These stars are then mapped into three dimensions and are then driven to an accurate numerical equilibrium by applying a velocity-dependent acceleration \vec{f}_{damp} while keeping the temperature constant. The stars are then placed at an initial separation that is large enough to avoid any immediate mass transfer. The full SPH code is then used to relax the initial conditions to a tidally deformed binary system at the brink of numerically resolvable mass transfer. This phase of the initialization is

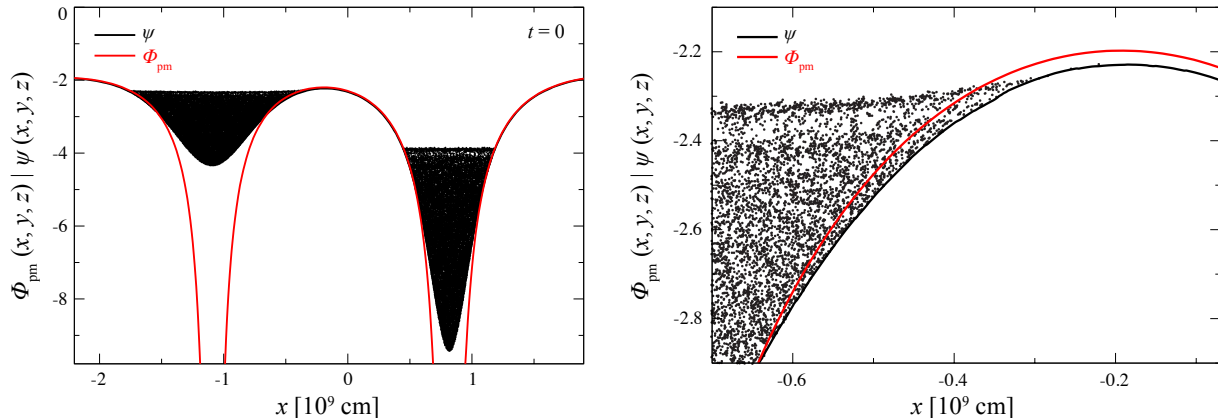


FIG. 3.— Projection of the SPH particles on the $(x, \Phi_{\text{pm}}/\Psi)$ plane. The dotted red line is the point mass Roche potential, $\Phi_{\text{pm}}(x, y = 0, z = 0)$. The solid black line is the value of the potential Ψ along the x -axis, the SPH particle values are shown as filled black circles. *Left:* Wide view showing both stars. *Right:* Zoom into the neighborhood of the Lagrange point L_1 . The fluid potential Ψ lies below the point mass value Φ_{pm} and therefore the point mass approximation underestimates the distance where mass transfer sets in, performed in a corotating frame, i.e. centrifugal and Coriolis forces must be accounted for³. We calculate the orbital frequency ω in a way that the total forces on the individual stellar centers of mass vanish exactly (Rosswog et al. 2004) and thus account for finite size deviations from the Kepler frequency. The acceleration applied to a particle i then reads

$$\mathbf{f}_i = \mathbf{f}_{\text{grav},i} + \mathbf{f}_{\text{hyd},i} - \boldsymbol{\omega} \times (\boldsymbol{\omega} \times \mathbf{r}_i) - 2\boldsymbol{\omega} \times \mathbf{v}_i - \frac{\mathbf{v}_i - \boldsymbol{\Omega}_{1,2} \times (\mathbf{r}_{1,2} - \mathbf{r}_i)}{\tau_i}. \quad (7)$$

Here, $\mathbf{f}_{\text{grav},i}$ and $\mathbf{f}_{\text{hyd},i}$ are the gravitational and hydrodynamic acceleration, \mathbf{r}_i and \mathbf{v}_i position and velocity in the corotating frame, $\boldsymbol{\Omega}_{1,2}$ is either the primary or the secondary star's angular velocity, and τ_i a damping time scale. In this frame, $\boldsymbol{\Omega}_{1,2} = 0$ for synchronized systems and $\boldsymbol{\Omega}_{1,2} = -\boldsymbol{\omega}$ for non-spinning stars. During this relaxation process, we adiabatically decrease the orbital separation a in a way that the orbital shrinkage time scale, $\tau_{\text{shrink}} = a/\dot{a}$, is substantially longer than dynamical timescale of the secondary $\tau_{\text{dyn},2}$,

$$\tau_{\text{shrink}} = \frac{a}{\dot{a}} = \frac{1}{\epsilon \sqrt{G\rho_2}} \gg \tau_{\text{dyn},2}, \quad (8)$$

where $\bar{\rho}_2$ is the average density of the secondary. We found that spurious oscillations are minimized for values of $\epsilon \lesssim 0.05$. As soon as the first SPH particle crosses the Lagrange point L_1 , we stop the relaxation process, transform to a space-fixed frame with the same coordinate origin and start the dynamical simulation. This moment is adopted as the time origin ($t = 0$) of the simulation, shown in Figure 2 for a $0.9 + 1.2 M_{\odot}$ system. In Figure 3 we show the potential of the initial conditions, where Φ_{pm} is the usual Roche potential as calculated for a point mass binary,

$$\Phi_{\text{pm}}(\mathbf{r}) = -\frac{GM_1}{|\mathbf{r} - \mathbf{r}_1|} - \frac{GM_2}{|\mathbf{r} - \mathbf{r}_2|} - \frac{1}{2}(\boldsymbol{\omega}_k \times \mathbf{r})^2 \quad (9)$$

with M_1/M_2 and $\mathbf{r}_1/\mathbf{r}_2$ the stellar masses and centre of mass positions and $\boldsymbol{\omega}_k$ the point mass Kepler frequency. The quantity Ψ is the corresponding quantity as calculated for the actual fluid configuration

$$\Psi(\mathbf{r}) = \Phi(\mathbf{r}) - \frac{1}{2}(\boldsymbol{\omega} \times \mathbf{r})^2, \quad (10)$$

where $\boldsymbol{\omega}$ is the orbital frequency of our (fluid) binary and Φ the gravitational potential due to the fluid.

As we will show below in detail, the accuracy of the initial conditions has a strong impact on all major aspects of the simulations, prolonging the mass transfer stage by dozens of orbits in all investigated cases.

3.2. Numerical treatment

In this section we explore the sensitivity of the binary evolution on physical and numerical factors, including numerical resolution, shock heating treatment, the artificial viscosity prescription, and the initial conditions.

3.2.1. Dependence on numerical resolution

The duration of mass transfer and the separation at which it begins depends on the extent to which we can resolve the outer layers of the WD donor. In SPH, where usually the particle masses are not evolved in time, this means that even in a decent numerical effort with a million SPH particles the initial resolvable mass transfer rate is already a substantial fraction of the total system mass. The numerically resolvable mass transfer \dot{M}_{lim} can be estimated as

$$\dot{M}_{\text{lim}} \approx \frac{1 \text{ particle mass}}{\text{orbital period}} \approx 2 \times 10^{-8} \left(\frac{N_p}{10^6}\right)^{-1} \left(\frac{M_{\text{tot}}}{1 M_{\odot}}\right)^{3/2} \left(\frac{a_0}{2 \times 10^9 \text{ cm}}\right)^{3/2} \frac{M_{\odot}}{\text{s}}, \quad (11)$$

³ As the velocities vanish for synchronized systems, Coriolis forces can (and should) be ignored in this case to reach equilibrium faster.

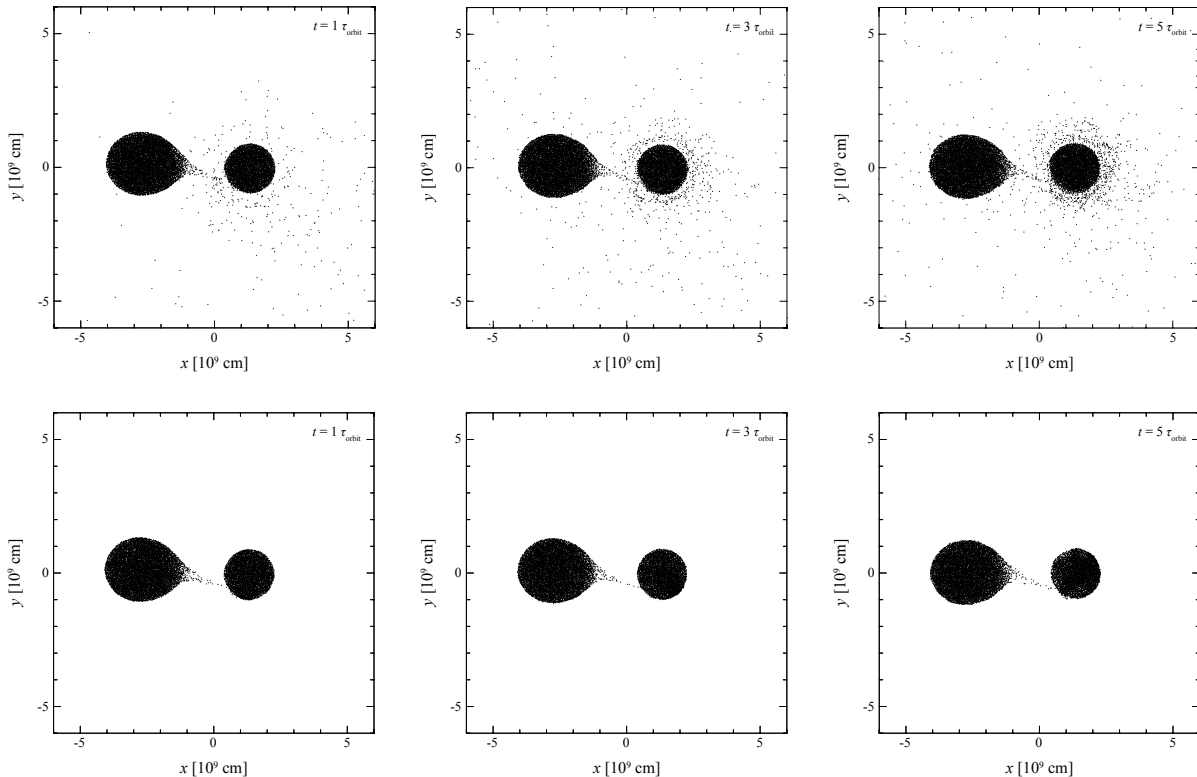


FIG. 4.— Particle distribution for a test run with (upper row) and without (bottom row) shock heating. Shown are snapshots after 1, 3 and 5 orbital periods.

where a_0 is the separation between the stars at the onset of mass transfer. In order to better resolve regions of lower density, SPH particles of different masses could be used, but we refrain from such a possibility as it can introduce a substantial level of numerical noise.

3.2.2. Comparison with the StarCrash code

As a validation of our code we have also performed a comparison with the results obtained with the StarCrash code. This code was developed originally by Rasio and Shapiro to study merging binaries (Rasio & Shapiro 1992, 1994, 1995). The major conceptual difference in their code is the use of a fast Fourier transform instead of a tree to calculate the gravitational forces.

To enable a valid comparison, for this test we also use a polytropic EOS, $P = K\rho^{5/3}$, with $\Gamma = 5/3$, we evolve the entropic function according to

$$\frac{dK_i}{dt} = \frac{\Gamma - 1}{2\rho_i^{\Gamma-1}} \sum_j m_j \Pi_{ij} \mathbf{v}_{ij} \cdot \nabla_i W_{ij}, \quad (12)$$

where m_j is the mass of particle j , Π_{ij} the artificial viscosity tensor depending on parameters α and β , $\mathbf{v}_{ij} \equiv \mathbf{v}_i - \mathbf{v}_j$ the velocity difference between particle i and j , and W is the smoothing kernel. We fix our artificial viscosity parameters in this comparison to the values recommended in their StarCrash documentation ($\alpha = 0.5$, $\beta = 1$). We use the subroutines of the StarCrash code to set up a synchronized binary system of mass ratio $q = 0.5$ with 40,000 SPH particles, both simulations start from these initial conditions. The codes yield nearly indistinguishable results, after about 15 orbital periods the donor WD becomes tidally disrupted. Although Rasio & Shapiro (1995) also utilizes the StarCrash code, they start with slightly different initial conditions, with the two stars being closer to one another at $t = 0$. As a result, they find that the donor only survives 5 orbits, despite using the same EOS and SPH particle number. We suspect that they started from a slightly too small initial separation, but the very good agreement of the two codes for the same initial conditions is encouraging. In passing we note that these results are very similar to those D'Souza et al. (2006), which will be discussed in more detail in Section 4.4.

3.2.3. Effect of shock heating treatment

As mentioned previously, recent grid-based simulations (Motl et al. 2002; D'Souza et al. 2006; Motl et al. 2007) showed long-lived mass transfer phases, in contrast to the earlier SPH simulations. In these calculations artificial viscosity was only used in the momentum equation, but not in the energy equation, which means that entropy production in shocks was neglected. It was suspected that at least part of the difference in the mass transfer duration may be due to the suppression or emergence of shocks/ignoring the change of entropy (Fryer & Diehl 2008).

We perform two test calculations at the example of a $q = 0.5$ binary, similar to D'Souza et al. (2006). We follow their approach and use a $\Gamma = 5/3$ -polytrope, but in one case we evolve the entropic function according to Equation

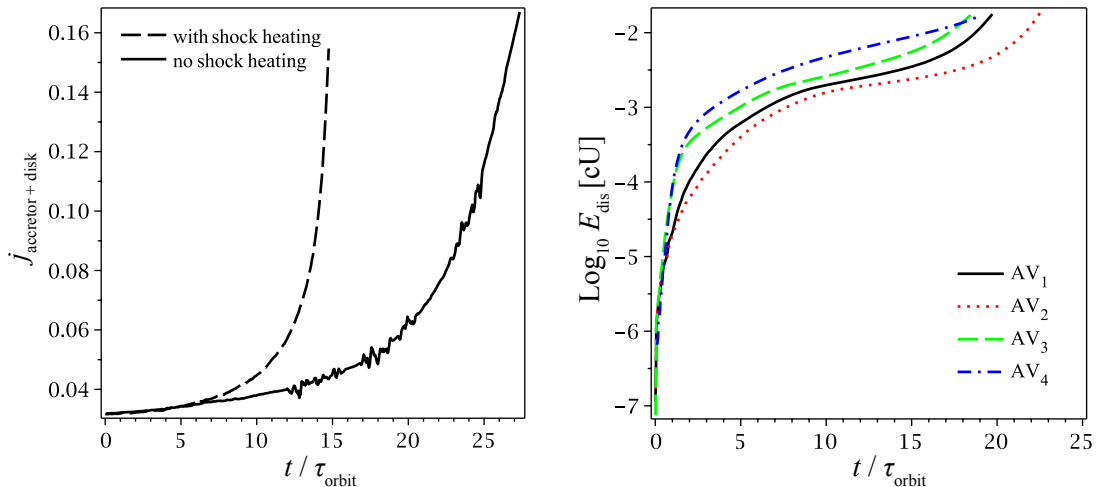


FIG. 5.— Left: specific angular momentum evolution (of accretor plus disk) for the test case where we explore the effect of the (non-)inclusion of shock heating onto the orbital evolution. Right: evolution of the total energy dissipated, E_{diss} , by the different artificial viscosity prescriptions. See text for details. Time is measured in units of the initial orbital period, τ_{orbit} .

(12) and in the other we keep K constant. A mass ratio of 0.5 results in a direct impact of the accretion stream onto the accretor surface. In the setup that does not include shocks, the accreted matter is smoothly incorporated into the accretor (Figure 4, lower row), while the setup that includes shocks produces a high-entropy halo around the accretor (Figure 4, upper row). This high-entropy halo applies a greater torque on the binary as it has a larger effective lever arm than the low-entropy halo that is produced when shocks are neglected. As a result, the matter within the high-entropy halo is able to remove more angular momentum from the orbit over the same number of orbital periods (Figure 5), leading to a more rapid evolution of the binary separation. This supports the findings of Fryer & Diehl (2008) that the large increase in orbital separation reported by D’Souza et al. (2006) is in part an artifact of shock suppression.

3.2.4. Impact of the artificial viscosity prescription

As we have shown that the entropy generation associated with shocks can affect the stability of double degenerate systems, we need to consider the importance of other entropy-generating mechanisms. To this end we compare different implementations of artificial viscosity. All have the “standard” form originally suggested by Monaghan & Gingold (1983), but differ in terms of constant or non-constant parameter values and additional “limiter switches”:

- AV_1 : constant parameters $\alpha = 1$ and $\beta = 2$
- AV_2 : constant parameters $\alpha = 2$ and $\beta = 4$
- AV_3 : time-dependent parameters (Morris & Monaghan 1997), controlled as described in Rosswog et al. (2008), but without “Balsara switch” (Balsara 1995)
- AV_4 : time-dependent parameters plus Balsara switch as described in Rosswog et al. (2008).

As test case we run simulations with a 0.3 He and a 0.6 CO WD, each one modeled by 20,000 particles (T4-T7, Table 1). Synchronized initial conditions are constructed as described in Section 3.1.2 and all tests used the Helmholtz EOS. Artificial viscosity does indeed have an impact: in the lowest viscosity case, AV_4 , the system merges after 19, in highest-viscosity case, AV_2 , after 22 orbital periods. To quantify the dissipation we calculate the thermal energy produced by artificial viscosity before merger

$$E_{\text{diss}} = \sum_i m_i \int_0^t \left(\frac{du_i}{dt} \right)_{\text{diss}} dt', \quad (13)$$

where

$$\left(\frac{du_i}{dt} \right)_{\text{diss}} = \frac{1}{2} \sum_j m_j \Pi_{ij} \mathbf{v}_{ij} \cdot \nabla_i W_{ij} \quad (14)$$

is the artificial viscosity contribution to the energy equation of particle i . The quantity E_{diss} as a function of time (for $t < t_{\text{disr}}$ where t_{disr} is the time when the donor star is tidally disrupted) is shown in Figure 5 (right panel), for all four artificial viscosity prescriptions. Interestingly, the prescription with the lowest average artificial dissipation parameters, AV_4 , dissipates the most energy. The reason for this is that the combination of low viscosity parameters and low resolution allow the SPH particles to build up a large level of velocity noise (i.e. fluctuations around the local average value). This leads to an increase in the typical value of \mathbf{v}_{ij} , and thus more dissipation, despite the lower viscosity parameters and suppression of dissipation in shear flows.

The increased rate of dissipation results in a more efficient spin-up of the accretor, with the angular momentum for this spin-up coming at the orbit’s expense. This leads to a reduction in the number of orbital periods the binary can survive prior to merger. We perform our production runs with prescription AV_4 which yields a lower limit on the duration of the mass transfer phase.

3.2.5. Dependence on initial conditions

As we have discussed, most of the earlier WD merger simulations were constructed using approximate initial conditions where the separation was estimated by comparison of the stellar radius with the Roche lobe size. To illustrate the importance of carefully constructed initial conditions, here we compare the evolution of a binary initialized using both “approximate” and “accurate” initial conditions (ICs).

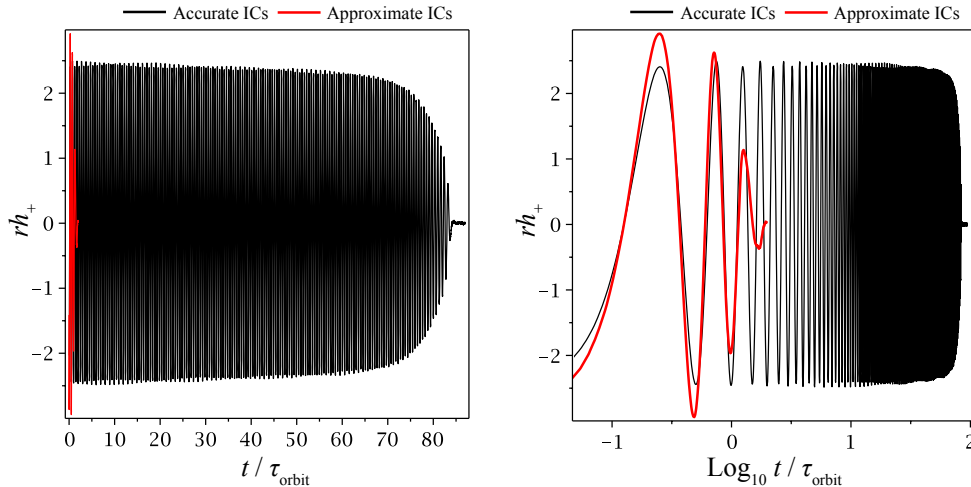


FIG. 6.— Gravitational wave amplitude h_+ for the $0.2 + 0.8 M_{\odot}$ system (r is the distance to the observer) as a function of time in units of the initial orbital period of the system, τ_{orbit} , both with “approximate” (red) and “accurate” ICs (black).

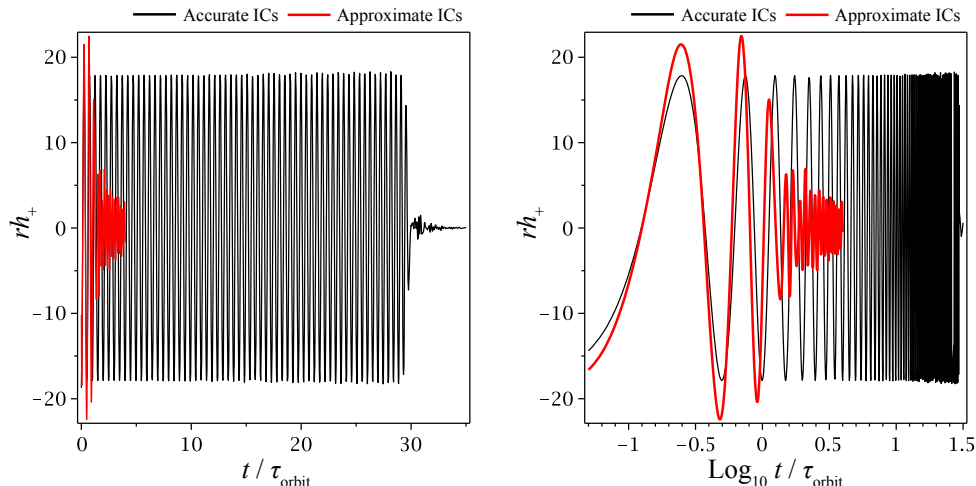


FIG. 7.— Same as Figure 6, but for the $0.6 + 0.9 M_{\odot}$ system.

To construct the approximate ICs, we equate Eggleton’s formula (Eggleton 1983) for the Roche radius with the radius R_2 of the secondary as found from the SPH particle positions. The initial separation a_0 is thus given by

$$a_0^{\text{Egg}} = R_2 \frac{0.6q^{2/3} + \ln(1 + q^{1/3})}{0.49q^{2/3}}. \quad (15)$$

The stars, previously relaxed in isolation (i.e. without the companion’s tidal field), are subsequently placed at this mutual separation with a spin that has the same period as the orbit of the binary. We refer to these ICs as “approximate” and compare them to the carefully constructed ICs described in Section 3.1.2. The described procedure is plausible, as we will see below, its approximate nature introduces a slew of artifacts.

Two representative examples of binaries are compared, a $0.2 M_{\odot}$ He + $0.8 M_{\odot}$ CO binary and a $0.6 M_{\odot}$ CO + $0.9 M_{\odot}$ CO binary. Each system is simulated using both the approximate (corresponding to runs T1 and T2 in Table 1

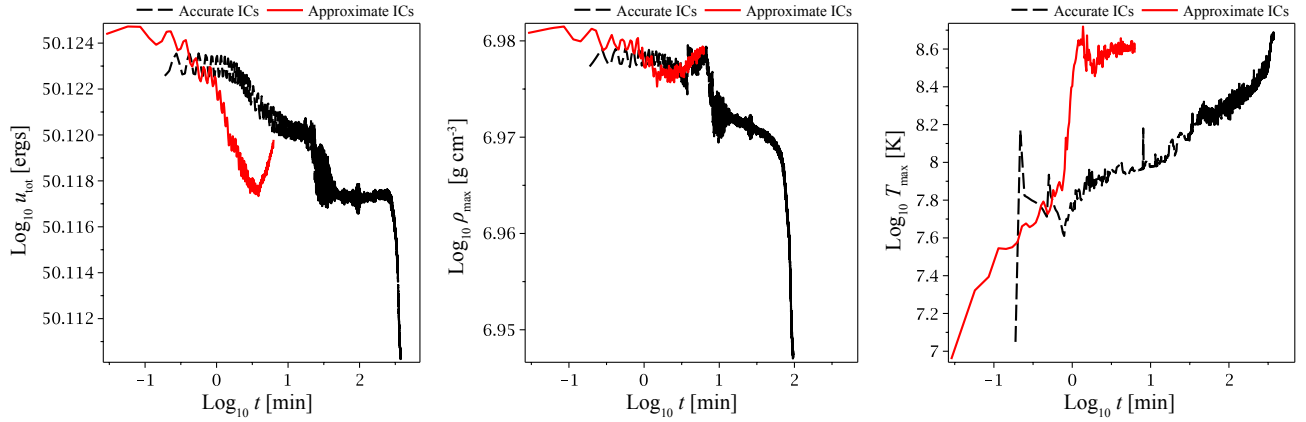


FIG. 8.— Evolution of thermodynamic quantities for a $0.2+0.8 M_{\odot}$ system both with approximate (red) and accurate ICs (black). Shown are: total internal energy (left), maximum density (center) and temperature (right) as a function of time t in units of minutes.

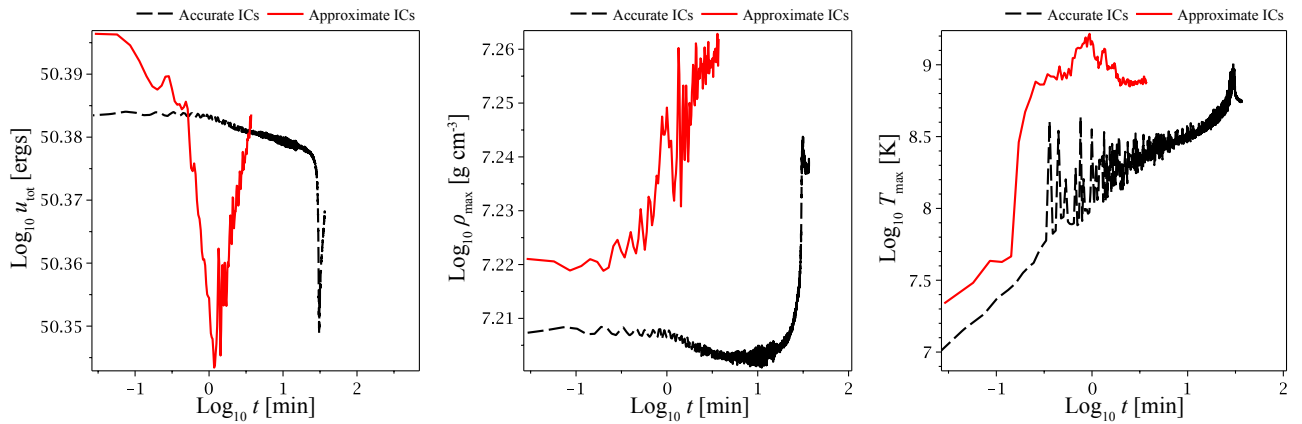


FIG. 9.— Similar to Figure 8 but for the $0.6+0.9 M_{\odot}$ system.

and Figure 1) and accurate (P1 and P5) ICs. Some marked differences are seen between the simulations initialized using these two different prescriptions. The approximate prescription systematically underestimates the separation at which mass transfer sets in by about 14% in both cases. This is mainly because it neglects the tidal deformation of the donor star. As a result, binaries initialized using approximate ICs carry a deficit of angular momentum when compared to those evolved using the more accurate prescription. The difference in angular momentum between the two IC prescriptions is 11% and 13% for the $0.2+0.8 M_{\odot}$ and $0.6+0.9 M_{\odot}$ cases, respectively. This slight discrepancy severely impacts their subsequent evolution, with the duration of the mass transfer phase being underestimated by about two order of magnitude. In the $0.2+0.8 M_{\odot}$ case, the approximate ICs yield two orbits (478 s) of mass transfer while the accurate ICs show a mass transfer for as long as 84 orbital periods (20,328 s). The difference in the $0.6+0.9 M_{\odot}$ case is similarly dramatic (1 vs 29 orbital periods).

The effect of varying ICs on the orbital dynamics is most clearly seen when comparing the resulting gravitational wave signals (Figures 6 and 7). The approximate ICs give rise to a rapidly fading signal, while in the more accurate case the amplitude remains essentially constant up to the point of tidal disruption. The $0.6+0.9 M_{\odot}$ case, which is less stable than the $0.2+0.8 M_{\odot}$ system (Figure 1), shows only a slightly noticeable increase in the gravitational wave amplitude up to disruption. In both cases, the approximate ICs overestimate the peak amplitude and frequency. The approximate case gives an orbital frequency of 46 mHz in the $0.6+0.9 M_{\odot}$ case and 10 mHz in the $0.2+0.8 M_{\odot}$ case, while the accurate ICs yield 38 and 8.4 mHz, respectively (a difference of about 20%). This is mainly due to the difference in separation at final plunging (40% difference for the $0.2+0.8 M_{\odot}$ case and 30% for the $0.6+0.9 M_{\odot}$ case).

As a result of the more abrupt artificial decrease in separation, the approximate initial conditions also give rise to large spurious oscillations of the central remnant core. Such oscillations are imprinted not only on the gravitational wave signal (see Figure 7) but are also present on the thermodynamical trajectories of the merger products. As shown in Figures 8 and 9, both peak densities and temperatures are overestimated when using the approximate ICs. The use of accurate ICs helps to better characterize the time evolution of the temperature, density, and angular momentum during mass transfer as well as the final morphology of the merger product, as seen in Figure 10. Due to the larger initial separation for the more accurate ICs, the matter possess more total angular momentum, which results in more mass in the trailing arm and less mass in the disk than when starting from the approximate IC. The material ejected on eccentric orbits will fall back later onto the remnant (similar to the case of neutron star mergers; see e.g. Rosswog 2007; Lee & Ramirez-Ruiz 2007), the timescale of this fallback matter being seriously underestimated when using the

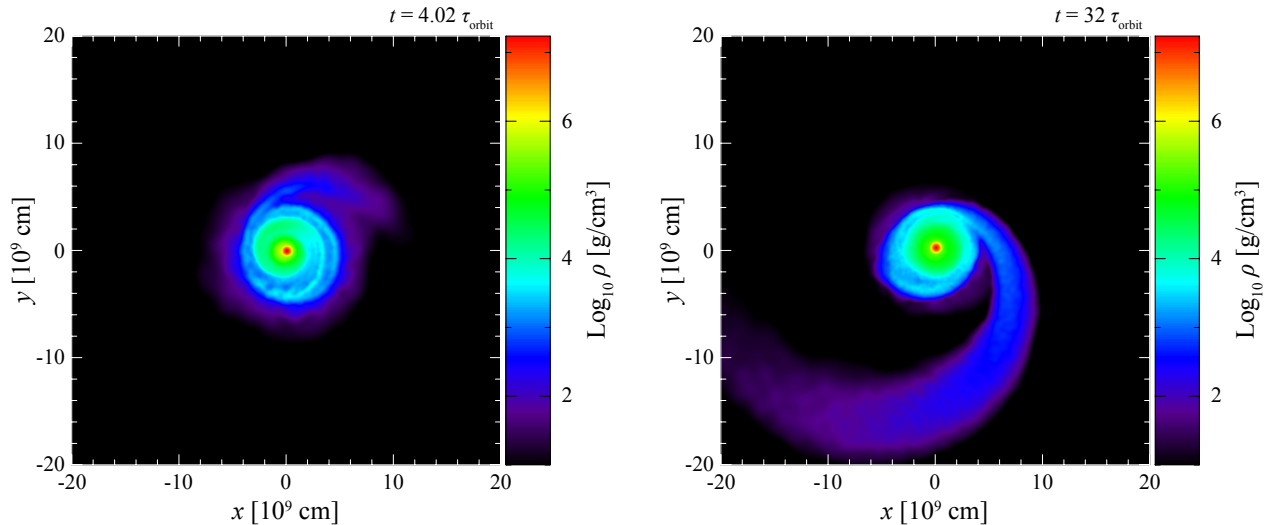


FIG. 10.— Remnant structure resulting from the merger of a $0.6 + 0.9 M_{\odot}$ binary system, captured 3 orbits after plunging. The left (right) panel shows the result for approximate (accurate) ICs. The initial angular momentum content in the system in this case differs by 13% between the two different IC prescriptions. This slight discrepancy severely impacts their subsequent evolution, with the duration of the mass transfer phase being severely underestimated by the approximate prescription. The approximate ICs yield one orbit before plunging while the accurate ICs show a mass transfer for as long as 29 orbital periods.

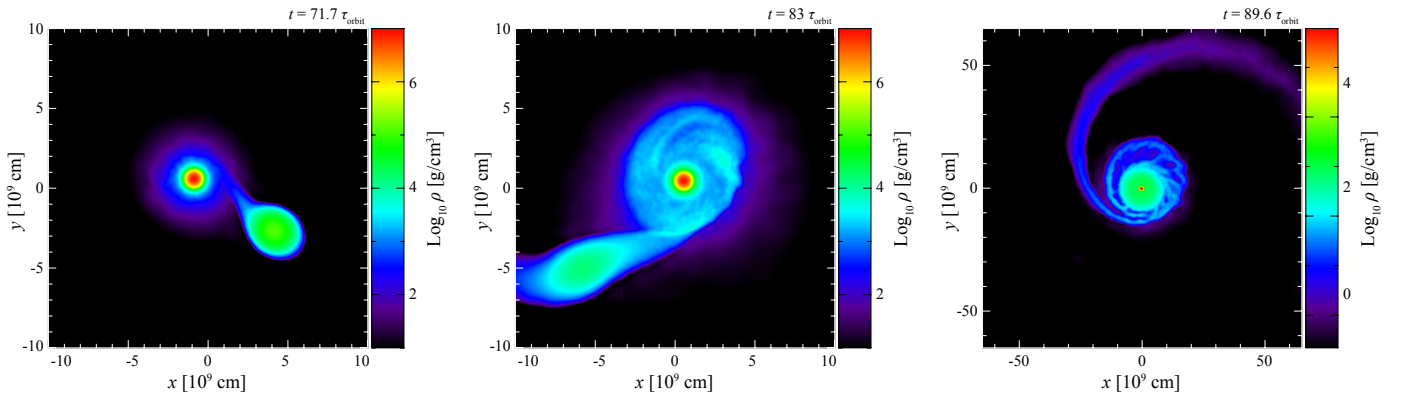


FIG. 11.— Dynamical evolution of a $0.2 M_{\odot}$ He and a $0.8 M_{\odot}$ CO WD (at 71, 83 and 89 times the initial orbital period). The mass transfer in this system continues for as long as 84 orbital periods until the He WD is finally destroyed. Times are shown in the upper right corner of each frame in units of the initial orbital period.

approximate ICs.

4. WHITE DWARF MERGER SIMULATIONS WITH ACCURATE INITIAL CONDITIONS

The use of accurate initial conditions and a correct treatment of shock heating is necessary for a reliably temporal evolution of the temperature, density, and angular momentum during the mass transfer phase. The evolution of two representative binary systems is described here in detail: the merger of a synchronized binary system with a $0.2 M_{\odot}$ He WD and a $0.8 M_{\odot}$ CO WD (P1, Table 1) and a tidally locked binary with $0.6 + 0.9 M_{\odot}$ CO WDs (P5). Their evolution is then subsequently compared with the wide range of binary systems that we have simulated as well as with the results of earlier work.

4.1. $0.2 + 0.8 M_{\odot}$: A borderline unstable system near the disk stability limit

According to the stability analysis of Marsh et al. (2004) a $0.2 M_{\odot}$ He + $0.8 M_{\odot}$ CO M_{\odot} binary system (marked as “P1” in Figure 1) should still be in the “direct impact” regime where the pericentre separation of the transferred mass is smaller than the accretor radius, but near the stable, disk forming regime. This is clearly seen in simulation snapshots of the matter distribution plotted in Figure 11. In this case, we find that the rotation of the donor star remains synchronized with the orbital motion throughout the mass transfer phase up to the point of tidal disruption. More importantly, as soon as mass transfer sets in, the orbit is observed to become rapidly eccentric and the mutual stellar separation begins to oscillate (with about 5% amplitude changes), see Figure 12. This oscillation, as expected, also modulates the mass transfer rate (Figure 12).

The average orbital separation in this system is observed to secularly increase and, as a result, the mass transfer is stabilized, similar to what is expected for AM CVn stars. The transfer rate stays nearly constant at a level of $\approx 10^{6.2} M_{\text{Edd}}$ for about 50 orbital periods and continues until the donor star is completely disrupted. This occurs after as many as 84 orbital or 16,930 dynamical time scales of the accretor. Before being disrupted, the donor star loses about

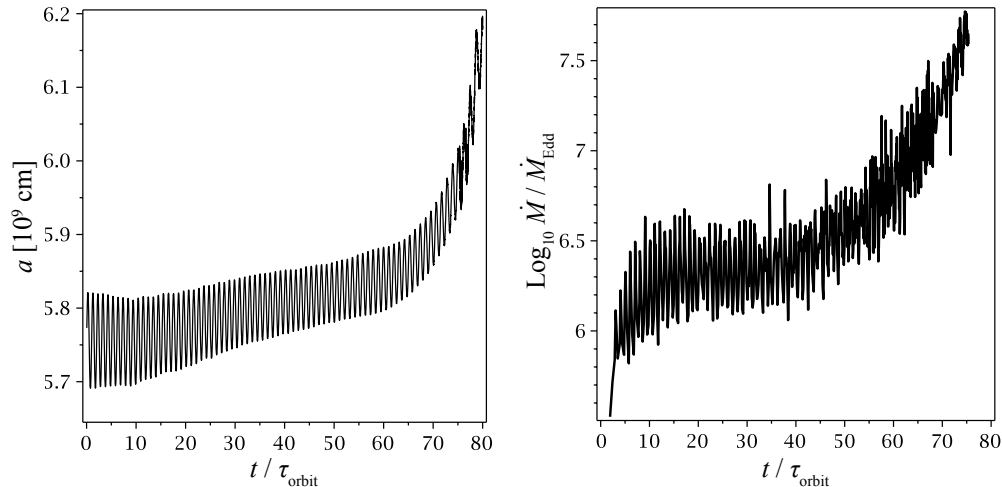


FIG. 12.— Evolution of orbital separation (in 10^9 cm; left) and mass transfer rate (in units of the Eddington value; right) of the $0.2+0.8M_{\odot}$ binary, P1 in Table 1.

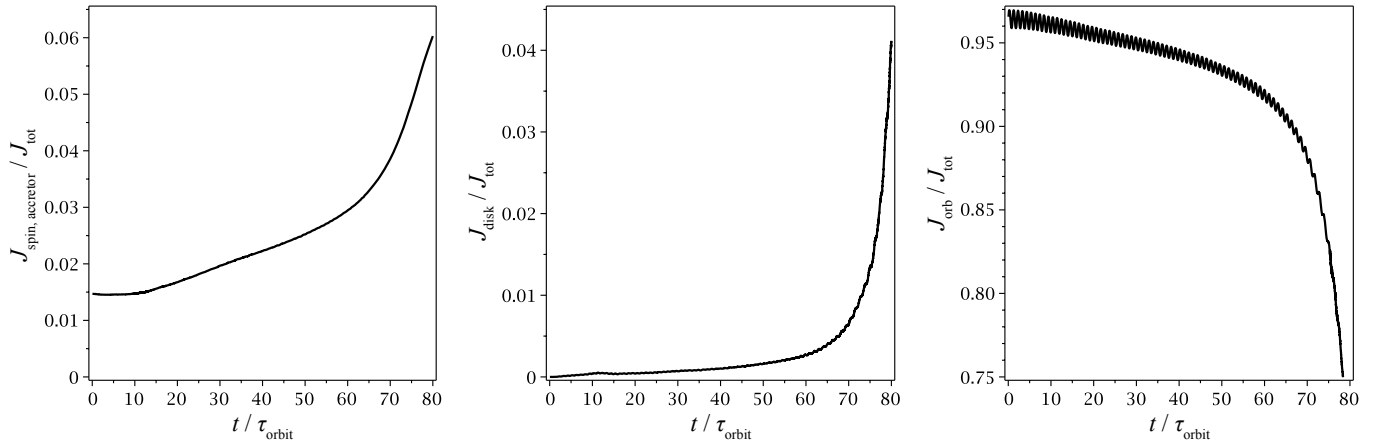


FIG. 13.— Evolution of spin, disk and orbital angular momentum of the $0.2+0.8 M_{\odot}$ case (P1 in Table 1). J_{tot} is the initial total angular momentum of the system.

$0.08 M_{\odot}$. Our results are in agreement with the Marsh et al. analysis, which suggests the mass transfer phase to be long-lived but still unstable.

The binary system during the mass transfer phase sheds matter through the outer Lagrange points, resulting in the loss of approximately 4% of the total angular momentum. As we have argued, the orbital dynamics is very sensitive to the loss of angular momentum which, in turn, prevents efficient mass transfer stabilization. The orbital angular momentum that is carried away is shared between the accreting star and the disk (Figure 13), and, due to the constant change in orbital separation, is observed to oscillate (Figure 13).

The densities and temperatures of the final remnant core are shown in Figure 14 for the $0.2+0.8 M_{\odot}$ case. The highest temperatures are reached in the shearing region between the central core and the surrounding thick disk. The peak temperatures of around 4×10^8 K are reached at densities of only about 10^5 g cm^{-3} , so that no efficient carbon burning is expected to occur.

4.2. $0.6+0.9 M_{\odot}$: An unstable binary system with direct impact mass transfer

A $0.6+0.9 M_{\odot}$ binary system is predicted to be in the unstable, direct impact regime (P5 in Figure 1). This is seen in the three dimensional density renderings plotted in Figure 15, which show the binary system at three different stages of its merger evolution. Although clearly unstable, the mass transfer continues for about 29 orbital periods before disruption. In contrast to the $0.2+0.8 M_{\odot}$ case, the orbit systematically shrinks from the onset of the mass transfer phase (Figure 16) and shows no noticeable oscillations. The depletion of the donor star in the $0.6+0.9 M_{\odot}$ and $0.2+0.8 M_{\odot}$ binary systems is shown in Figure 17. In the $0.2+0.8 M_{\odot}$ case, the donor mass decreases very regularly to about 90%, followed by a phase where the mass loss speeds up dramatically and the donor becomes subsequently disrupted during the remaining 20 orbits. Once mass transfer begins in the $0.6+0.9 M_{\odot}$ case, the rate of mass loss from the donor star increases exponentially with time, leading to a swift depletion of the donor.

The motion of the SPH particles within the Roche-type potential Ψ (see Equation 10) are shown in Figure 18. As expected from a direct impact configuration, the angular momentum carried across is efficiently converted into the spin of the accreting star (Figure 19), with a small fraction being stored in the accretion torus. Similar to the $0.2+0.8$

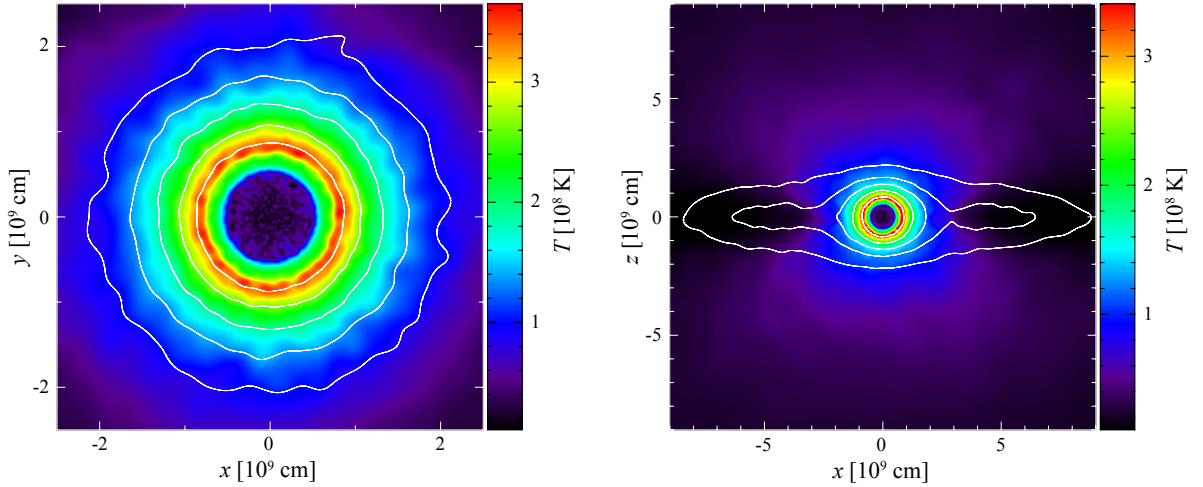


FIG. 14.— Densities and temperatures of the final remnant resulting from the merger of $0.2 + 0.8 M_{\odot}$ binary (P1): xy -plane (left) and xz -plane (right). Color-coded is the temperature (in units of 10^8 K), the overlaid white contours refer to $\log \rho$ (ρ in g cm^{-3}). The contours in the left panel show densities ranging from $\log_{10} \rho = 4$ (innermost contour) to $\log_{10} \rho = 2$ (outermost contour) in steps of 0.5, while the contours in the right panel range from $\log_{10} \rho = 4.1$ to $\log_{10} \rho = 2.9$ in steps of 0.3.

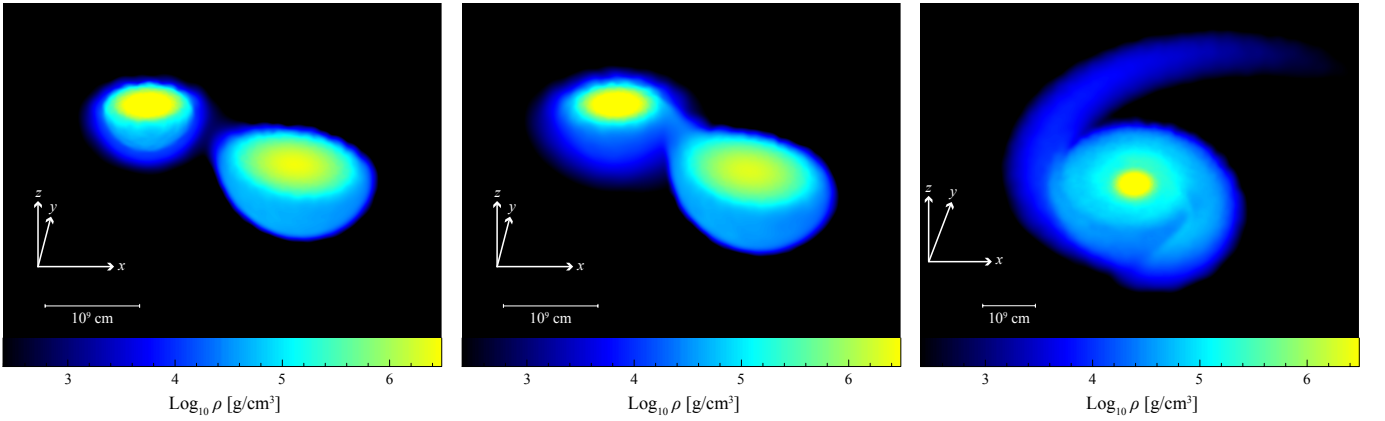


FIG. 15.— Evolution of the dynamically unstable system of two CO white dwarfs with $0.6 + 0.9 M_{\odot}$. The panels show three-dimensional renderings of the density at 16, 27 and 30 times the initial orbital period.

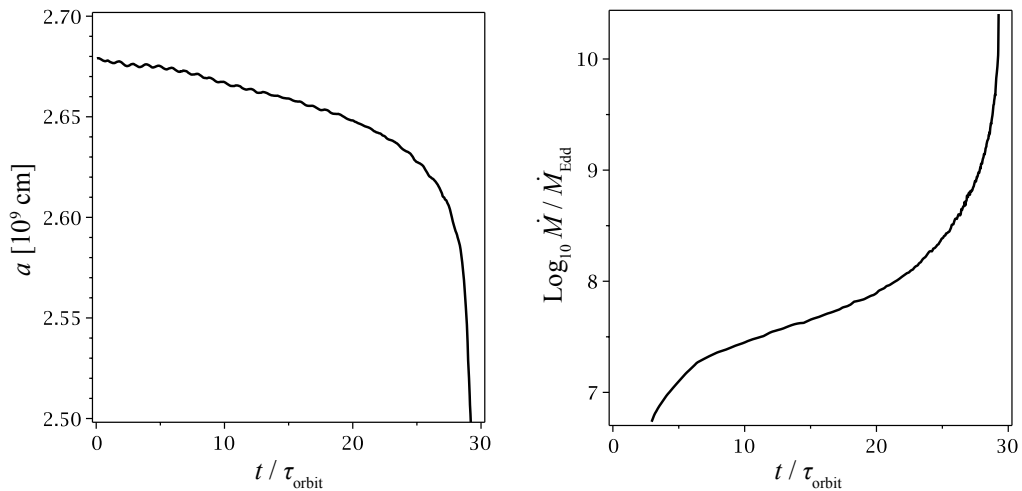


FIG. 16.— Orbital separation (in 10^9 cm; left) and mass transfer rate (in units of the Eddington value: right) for the unstable $0.6 + 0.9 M_{\odot}$ system, P5 in Table 1.

M_{\odot} binary system, the donor star is observed to remain close to synchronization during the entire duration of the mass transfer phase.

The thermodynamical properties of the remnant core are displayed in Figure 20. The peak temperatures now reach about 5×10^8 K at densities of about 10^6 g cm^{-3} . Under these conditions, carbon burning is observed to occur, but

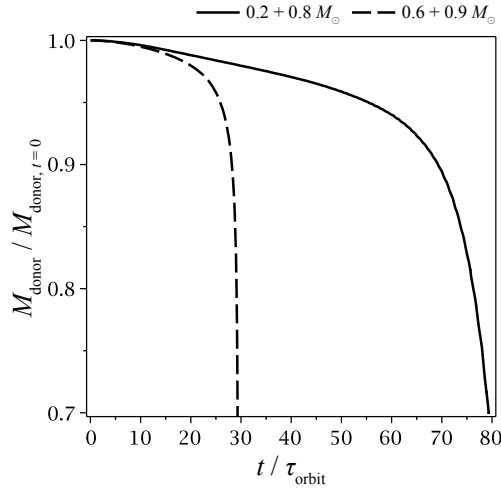


FIG. 17.— Evolution of the donor mass normalized to its initial value for both the $0.2 + 0.8$ (P1) and $0.6 + 0.9 M_{\odot}$ case (P5).

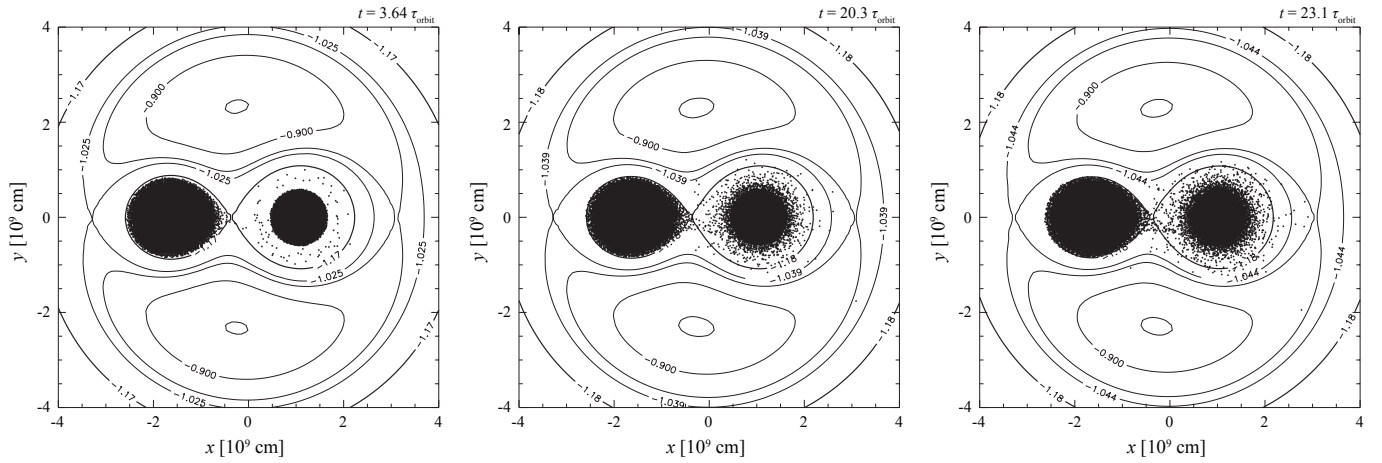


FIG. 18.— Roche contours for the system with $0.6 + 0.9 M_{\odot}$ components. Snapshots are taken after 3, 20 and 23 times the initial orbital period.

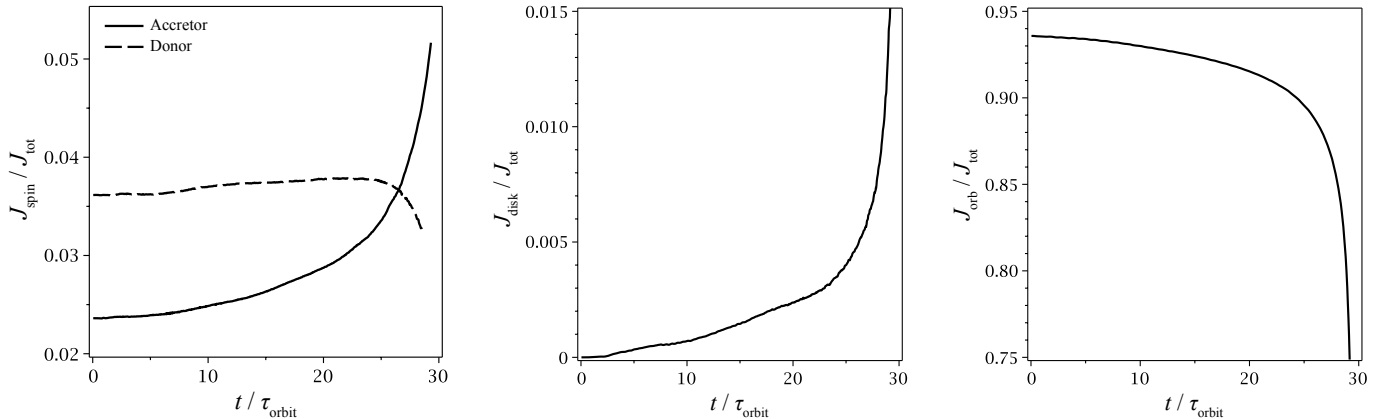


FIG. 19.— Dynamical evolution of the $0.6 + 0.9 M_{\odot}$ binary system. From left to right we have plotted the spin, disk and orbital angular momentum (normalized to the initial total angular momentum of the system: J_{tot}), respectively.

the rate of energy injection is not large enough to be dynamically dominant. The structure and further evolution of our double degenerate merger remnant products will be discussed in more detail elsewhere.

4.3. Summary of all other simulations

All the systems that we have simulated in this paper belong to the regime of direct impact, unstable mass transfer. In all cases, we find the mass transfer to survive for many orbits. For those close to the guaranteed stable disk regime (see Figure 1) the mass transfer phase extends for many tens of orbits. Systems belonging to these categories are represented here by our P1 ($0.2 + 0.8 M_{\odot}$) and P2 ($0.3 + 1.1 M_{\odot}$) simulations. The $0.3 + 1.1 M_{\odot}$ binary system shows

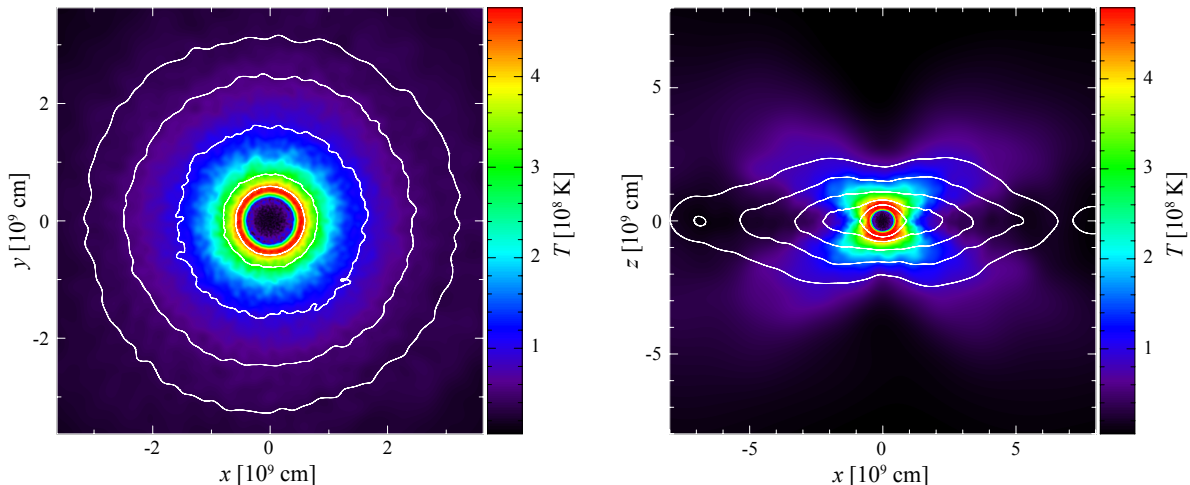


FIG. 20.— Densities and temperatures of the final remnants of the $0.6 + 0.9 M_{\odot}$ case (P5): xy -plane (left) and xz -plane (right). Color-coded is the temperature (in units of 10^8 K), the overlaid white contours refer to $\log \rho$ (ρ in g cm^{-3}). The contours in the left panel show densities ranging from $\log_{10} \rho = 5$ (innermost contour) to $\log_{10} \rho = 2$ (outermost contour) in steps of 0.75, while the contours in the right panel range from $\log_{10} \rho = 5.6$ to $\log_{10} \rho = 3.6$ in steps of 0.5.

a very similar evolution to the $0.2 + 0.8 M_{\odot}$ system described above. The mass transfer phase is stabilized, i.e. the rate of mass transfer does not increase exponentially but is observed to have a nearly constant mass transfer rate for many orbital periods.

The evolution of all other systems, which are far away from the limit of stable disk regime, is similar evolution to that of the $0.6 + 0.9 M_{\odot}$ binary system discussed above. In this case, a slow decrease in the separation is accompanied by a severe mass transfer rate increase. During the evolution, the donor star remains synchronized and the accretor is substantially spun up. All these systems lack stabilizing effects and are therefore prone to Kelvin-Helmholtz-triggered He-detonations at the accretor surface that were discussed in detail in (Guillochon et al. 2010) (see Section 6 for further details). Such systems could be possible candidates for sub-Chandrasekhar double detonation scenarios (Fink et al. 2007, 2010).

For all systems, we observe pronounced spiral arms extending out of the disk which engulfs the central remnant core. As we have discussed in Section 3.2.5 and shown in Figure 10, this feature may be much less pronounced in simulations that start from approximate ICs since they contain substantially less angular momentum. These cases do not settle into a quasi-steady-state. Instead the torques from accretor and tidal tail continue shaping the dynamical evolution of the disk, see e.g. Figure 11.

4.4. Comparison with other mass transfer calculations

The simulations of D’Souza et al. were the first to show that the binary system does not merge within few orbital time scales, but instead can survive for more than 30 orbital periods. These authors investigated the evolution of a polytropic system with mass ratio $q = 0.5$ starting from accurate initial conditions constructed in the framework of the self-consistent field technique. D’Souza et al. found an increase in the orbital separation and a concordant decrease of the mass transfer rate after about 20 orbital periods. After 32 orbits they had to stop their simulation due to the severe degradation of numerical conservation. At this stage, the binary system showed no sign of a pending merger. The authors experimented with a higher degree of contact of the same binary and consequently a higher initial mass transfer rate by extracting angular momentum at a rate of 1% per orbit. The merger is avoided even if the system is artificially driven together for three more orbits after it has reached contact. Only when driving is applied throughout the simulation, the donor is observed to get disrupted. This occurs after about 8 orbits.

We found that if we reduce the angular momentum at a 0.5%/orbit rate, the disruption process is 3 times shorter, compared when no driving is applied. For our $q = 0.5$ case ($0.3 + 0.6 M_{\odot}$, P4), for as long as we have the possibility to compare, we see a similar behavior to that of D’Souza et al. in both the orbital separation and the mass transfer rate. At the end, the donor star is, however, disrupted after 45 orbits of mass transfer.

The same authors also studied the evolution of a $q = 0.4$ system. They found a peak in the mass transfer rate after about 10 orbits followed by a rapid decrease. The authors stopped the simulation after 43 orbits, with no visible sign of a merger. From our calculations, P3 is the closest to their mass ratio (≈ 0.41). Our P3 simulation, however, shows a donor disruption after 31 orbits. This difference may be due to the different shock treatment and the different equation of state (Helmholtz vs. 5/3 polytrope).

5. GRAVITATIONAL WAVE SIGNALS

The Laser Interferometer Space Antenna (LISA) will provide the largest observational sample of (interacting) double white dwarf binaries (Farmer & Phinney 2003; Ruiter et al. 2010). Such systems enter the LISA observational window (0.1 mHz - 100 mHz) when they reach a period ≈ 5 hr. They subsequently secularly evolve through radiation reaction across the LISA band and are so numerous to create a stochastic foreground. When a binary reaches a gravitational

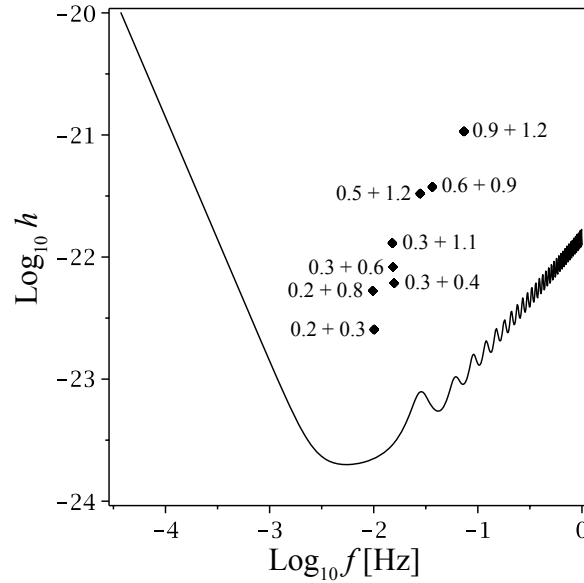


FIG. 21.— Gravitational wave amplitudes of the studied double WD systems for an assumed distance of 10 kpc. The overlaid curve shows the LISA sensitivity for a one-year integration period that has been produced with the online sensitivity curve generator from <http://www.srl.caltech.edu/~shane/sensitivity/>

wave frequency of a few mHz and is close enough to be resolved individually, the recorded signal shows an intrinsic frequency evolution over a typical one year observation time. Figure 21 shows the gravitational wave amplitudes (for an assumed distance of 10 kpc) for all our production runs together with the LISA sensitivity curve. Since none of the orbital frequencies change by more than 1 % in the last year prior to merger, we chose this as a typical integration time. Provided they are in the Milky Way, all of the investigated systems would be detectable by LISA.

We show that, depending primarily on the initial conditions, the frequency evolution of the binary can be calculated incorrectly. Simulations that use the approximate initial conditions, as discussed in Section 3.2.5, severely underestimate the initial separation when mass transfer sets in. As a result, the binary only survives for a few orbits resulting in a rapidly fading gravitational wave signal (see e.g. Figure 7). The accurate initial conditions, on the other hand, produce binary systems in which the mass transfer phase is dramatically extended by almost two orders of magnitude in time, resulting in a gravitational wave signal with amplitude and frequency that remain essentially constant up until merger. Population synthesis models have shown that these binaries are more numerous than dynamically stable systems for a given mass ratio (Nelemans et al. 2001b; Ruiter et al. 2010). As we show that these binaries can survive at small separation for hundreds of orbital periods (keep in mind our mass transfer duration estimates are –due to finite numerical resolution– strict lower limits on the durations realized in nature), their associated gravitational wave signal should be included when calculating the LISA gravitational wave foreground (although expected to be below LISA’s sensitivity at these high frequencies).

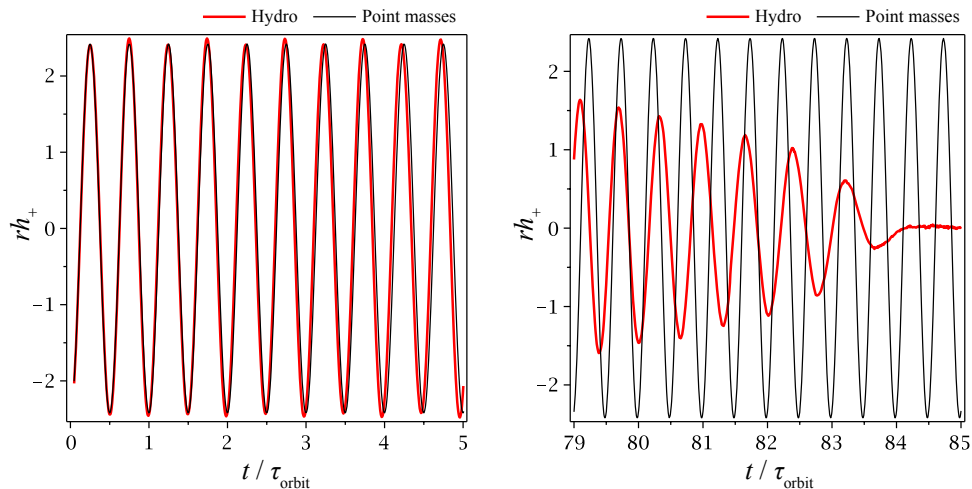


FIG. 22.— 0.2 He and 0.8 M_{\odot} CO WDs: comparison of the gravitational wave amplitude h_+ of the simulation with the point mass limit. r is the distance to the observer.

With the use of accurate initial conditions as well as realistic shock heating treatment, the frequency evolution of the binary can thus be explored in detail. Depending primarily on the mass ratio, as we have argued here, the resulting

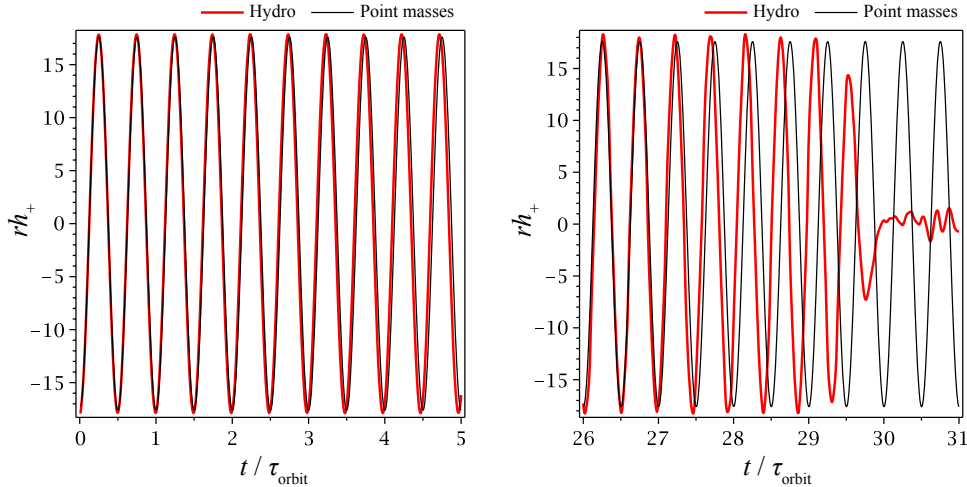


FIG. 23.— CO WDs with $0.6 + 0.9 M_{\odot}$: comparison of the gravitational wave amplitude h_+ of the full hydrodynamic simulation with the point mass limit. r is the distance to the observer and t is the time measured in units of the initial orbital period.

gravitational wave signal can be significantly different from that predicted in the point mass limit, particularly for marginally unstable systems. In such systems, the gravitational wave signal carries the imprint of the orbital oscillation, as illustrated by the evolution of the marginally unstable $0.2 + 0.8 M_{\odot}$ system in Figure 22.

For systems that are far from the stable disk limit, we find the point mass approximation to provide a better description of our simulated gravitational wave signals. This is mainly because the oscillations in the orbital separation are much less pronounced for these systems. Contrary to the $0.2 + 0.8 M_{\odot}$ case, the gravitational wave amplitude derived for the $0.6 + 0.9 M_{\odot}$ binary system remains close to the point mass prediction up to almost complete disruption, as seen in Figure 23.

6. SURFACE DETONATION CRITERIA IN WHITE DWARF BINARIES

During the final phase of mass transfer prior to merger, the rate of mass exchanged approaches the mass of the donor divided by the orbital timescale,

$$\dot{M}_2 \approx \left(\frac{M_2}{R_2} \right)^{3/2} \sqrt{\frac{G}{\mu_1}} \approx 0.1 M_{\odot} \text{ s}^{-1}, \quad (16)$$

where μ_1 is the reduced mass of the accretor. As shown in Guillochon et al. (2010), Kelvin-Helmholtz instabilities develop within the accretion stream once the accretor has built up a torus of material acquired from the donor, and this leads to the formation of dense knots of material that can periodically strike the accretor’s surface. This striking action can lead to the initiation of a detonation within the torus about the accretor, assuming that matter acquired from the donor mostly consists of helium.

The question of whether knots are capable of detonating the accretor’s helium layer depends on the ram pressure applied by individual knots, and by the initial conditions of the helium torus at the time of compression. From the SPH simulations presented in this paper we have an accurate record of the time-evolution of the accretion stream’s density at L1 and the conditions at the base of the helium torus. As shown in our FLASH simulations (Figure 25), a standing shock develops between the stream and the torus, equalizing the pressure at the stream-torus interface, and reducing the velocity of the fluid flow in the torus relative to the accretion stream to subsonic velocities. As the interaction is subsonic and no heat transport processes can operate effectively on a dynamical timescale, the accretion stream smoothly evolves relative to the background pressure, and thus maintains constant entropy. The exterior pressure experienced by the accretion stream is given by the pressure within the torus.

Given the initial density ρ_{L1} and temperature T_{L1} of the stream material as it leaves L1, the pressure at the base of the helium torus P_{tor} , and an equation of state that parameterizes the entropy s and pressure P as functions of density and temperature, we can determine the density of the stream when it reaches the base of the helium torus by solving the following system of equations for ρ_{knot} and T_{knot} ,

$$s(\rho_{L1}, T_{L1}) = s(\rho_{\text{knot}}, T_{\text{knot}}) \quad (17)$$

$$P(\rho_{\text{tor}}, T_{\text{tor}}) = P(\rho_{\text{knot}}, T_{\text{knot}}), \quad (18)$$

where “tor” refers to the base of the helium torus and “knot” refers to the stream post-compression. For all of the SPH simulations presented in this paper, the maximum increase in density achieved within the stream as it falls from L1 to the accretor’s surface is $\gtrsim 10$. The small initial entropy of the stream ($T_{L1} \sim 10^5$ K) and minimal shock-heating means that the final temperature reached within the stream is substantially smaller than the temperature required for dynamical burning, and thus burning is not expected to be important within the stream itself.

With our estimate for ρ_{knot} , we can estimate the increase in density and temperature of the torus after it is compressed by the stream. As in Guillochon et al. (2010), we solve for the trajectory of a test particle released at L1 with initial

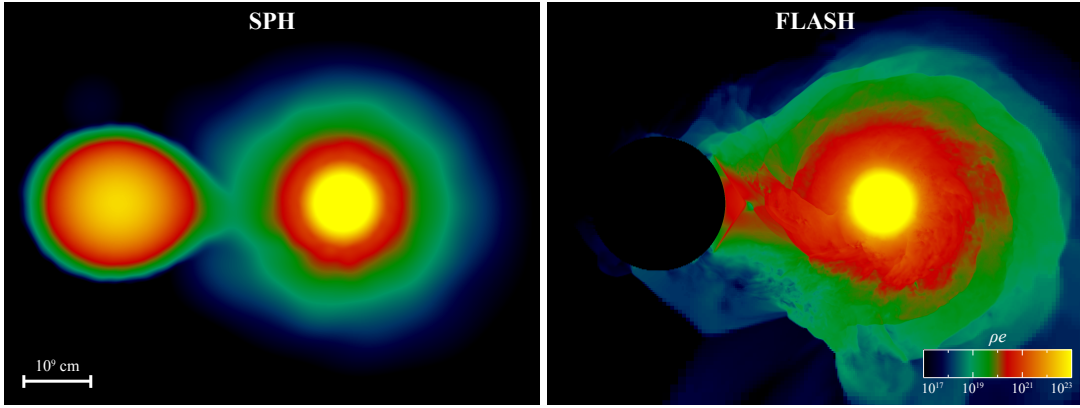


FIG. 24.— Side-by-side comparison of the fluid internal energy ρe for one of the SPH calculations featured in this work (G1) and one of the FLASH calculations of (Guillochon et al. 2010, run Ba) for a $0.45 + 0.9 M_{\odot}$ binary. The SPH calculation fully resolves both the donor and the accretor, which allows for the question of binary stability to be addressed self-consistently. However, the SPH calculation has limited resolution and is unable to sufficiently resolve the stream-torus interface, artificially suppressing the instabilities and the standing shocks that are observed to develop in the FLASH calculation. As a result of not resolving the standing shocks properly, the SPH calculation shows somewhat less heating in the torus than the FLASH calculation. On the other hand, the stream boundary condition used in the FLASH simulation is idealized to lie on the Roche surface of the donor, with a simplified initial velocity profile normalized to the sound speed of the donor, which does not perfectly represent the actual flow of material leaving L1.

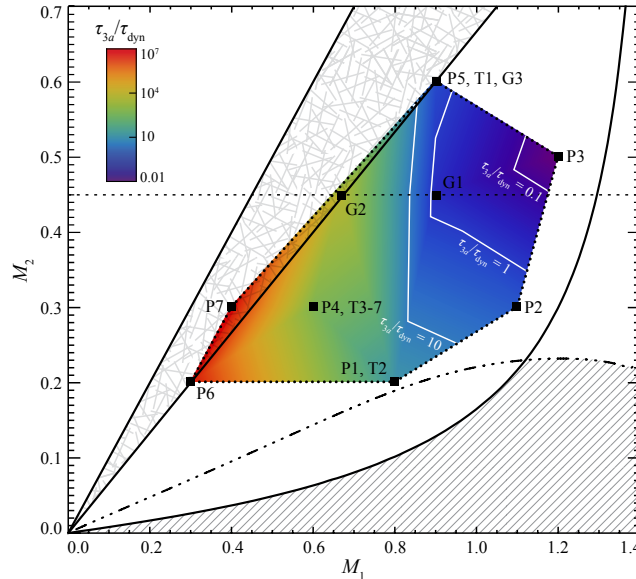


FIG. 25.— Ratio of the triple-alpha burning timescale $\tau_{3\alpha}$ to the dynamical timescale τ_{dyn} for different combinations of donor and accretor masses. The figure shows the same stability criteria as Figure 1, sans labels for clarity. The colored region shows the ratio of the two timescales, with the white contours showing where $\tau_{3\alpha} = 0.1\tau_{\text{dyn}}$, $\tau_{3\alpha} = \tau_{\text{dyn}}$, and $\tau_{3\alpha} = 10\tau_{\text{dyn}}$. The dotted line shows the convex hull of all simulations performed in which the donor can possess a significant amount of helium in its outer layers. For the two FLASH simulations performed in Guillochon et al. (2010) in which a surface detonation was observed (G1 and G3), the ratio of timescales is of order unity, whereas the simulation in which no detonation was observed (G2), $\tau_{3\alpha}$ is significantly larger than τ_{dyn} .

velocity given by the sound speed of the donor to estimate v_{\perp} , the component of the velocity perpendicular to the accretor’s surface. Given the density of the stream ρ_{knot} , we can determine the ram pressure of the stream

$$P_{\text{ram}} = \rho_{\text{knot}} v_{\perp}^2. \quad (19)$$

We can then use P_{ram} and solve a set equations similar to Equations (17) and (18) to determine the post-compression state of the torus

$$s(\rho_{\text{tor}}, T_{\text{tor}}) = s(\rho_{\text{comp}}, T_{\text{comp}}) \quad (20)$$

$$P_{\text{ram}} = P(\rho_{\text{comp}}, T_{\text{comp}}), \quad (21)$$

where “comp” refers to the conditions in the helium torus after compression. This enables us to calculate the triple-alpha burning timescale $\tau_{3\alpha}$ and compare it to the dynamical timescale τ_{dyn} at the accretor’s surface to determine if runaway burning can be achieved, leading in turn to a detonation.

In Figure 25 we show the curves for which $\tau_{\text{dyn}} = \tau_{3\alpha}$ and $10\tau_{\text{dyn}} = \tau_{3\alpha}$ within the convex hull of the SPH simulations presented in this paper. For the two simulations which exhibited surface detonations in Guillochon et al. (2010) the two

timescales are comparable, whereas t_{dyn} is far shorter than $\tau_{3\alpha}$ for the simulation that showed no surface detonation. The SPH simulations show that the conditions for dynamical burning being triggered on the surface of the accretor are achieved for accretor masses larger than $\sim 0.8M_{\odot}$, with a cutoff at low donor masses as the circularization radius of the accretion stream begins to exceed the radius of the accretor. Such systems could be possible candidates for sub-Chandrasekhar double detonation scenarios, as argued in Guillochon et al. (2010).

7. SUMMARY

The onset of (numerically resolvable) mass transfer in double degenerate binary systems and its impact on the orbital evolution forms the main theme of our paper. We find for all investigated cases that mass transfer ensues for at least dozens of orbits, even for systems which according to the analysis of Marsh et al. (2004) are guaranteed to be unstable. Due to the finite numerical resolution, the duration of the mass transfer phase calculated here should be considered as a strict lower limit.

Part of our motivation has been to settle a previous debate concerning the duration of mass transfer in such systems. Almost all of the earlier SPH simulations had found quick disruption of the donor star within a few orbital periods after the onset of mass transfer, while recent grid-based simulations (D’Souza et al. 2006) found a longer lived mass transfer phase. Using the same assumptions and initial conditions we have reproduced essentially all previous results. In addition we have compared our results to those obtained by using the StarCrash code developed by Faber and Rasio and found excellent agreement when using the same initial conditions and equation of state.

Concerning the mass transfer duration debate, we find that the reported discrepancies can be accounted for by the following two effects. The first is the self-consistent inclusion of entropy production in shocks, which we find to have a major impact on the orbital dynamics. In direct-impact systems, we find the realistic inclusion of shock heating to produce an extended, high-entropy halo around the accretor. When ignored, a smooth incorporation of the transferred material into the stellar surface is observed. Since substantial amount of angular momentum can be stored in the shocked material (which is provided at the expense of the orbital angular momentum), the realistic inclusion of shocks yields shorter lived mass transfer phases. These results confirm the earlier concerns raised by Fryer & Diehl (2008).

The second and even more important reason is attributed to the initialization procedure of the binary in the simulations. The results of simulations constructed using approximate corotating initial conditions have been compared with those using carefully constructed binaries and are found to be markedly different. Simulations that use the approximate initial conditions underestimate the initial separation at which mass transfer sets in by about 15%, which yields a binary that only survives for a few orbits and thus a rapidly fading gravitational wave signal. This is because once mass transfer sets in, the orbital evolution is no longer driven by angular momentum losses due to gravitational wave emission but instead is dominated by the redistribution of angular momentum in the system. The use of approximate initial conditions systematically underestimates the number of orbits and overestimates the gravitational wave peak frequencies and amplitudes by about 20 %. In contrast, the accurate initial conditions produce a binary system in which the mass transfer phase is extended by almost two orders of magnitude in time, resulting in a gravitational wave signal with amplitude and frequency that remain essentially constant up until merger. The mass transfer also shows a unique oscillatory signal that is most pronounced for binary systems that are near the disk forming limit.

The use of accurate initial conditions and a correct treatment of shock heating allows us to better characterize the time evolution of the temperature, density, and angular momentum, which are important when considering thermonuclear events that may occur during the mass transfer phase and/or after merger. Approximate initial conditions, for example, tend to significantly overestimate the densities and temperatures of the final merger remnant. This fact may have adverse consequences for possible type Ia candidate systems. Our treatment allows us to also accurately identify when surface detonations may occur in the lead-up to the merger. The results of this study have been used as boundary conditions for FLASH simulations that focus on the fate of the low-density accreted material and that are described in a companion paper (Guillochon et al. 2010). This combined study has shown that contrary to earlier beliefs, the mass transfer can be very eventful. We have shown that for the case of unstable, direct impact He accretion onto the accretor a hot ($> 5 \times 10^8$ K) helium torus builds up in which the incoming accretion stream triggers Kelvin-Helmholtz instabilities. Such Kelvin-Helmholtz “knots” repeatedly impact the accretor’s helium surface and, once the triple-alpha time scale is shorter than the local dynamical time scale, can trigger violent surface explosions. This explosion launches shocks into the accretor’s interior that can subsequently ignite the carbon oxygen core. This could possibly be the long sought-after explosion mechanism how to trigger supernova explosion in a double degenerate scenario which, together with the promising rates, could make double degenerate mergers a viable (sub-luminous) type Ia progenitor system.

We thank Lars Bildsten, Marcus Brüggen, Philipp Podsiadlowski, John Fregeau, Dan Kasen, Gijs Nelemans and Ken Shen for very useful discussions. We acknowledge support from DFG grant RO 3399 (M.D. and S.R.), the David and Lucille Packard Foundation (JG and ER-R), NSF grant: PHY-0503584 (ER-R), and the NASA Earth and Space Science Fellowship (JG).

REFERENCES

- Balsara, D. S. 1995, *Journal of Computational Physics*, 121, 357
 Benz, W., Cameron, A. G. W., Press, W. H., & Bowers, R. L. 1990, *ApJ*, 348, 647
 Clayton, G. C., Geballe, T. R., Herwig, F., Fryer, C., & Asplund, M. 2007, *ApJ*, 662, 1220

- D'Souza, M. C. R., Motl, P. M., Tohline, J. E., & Frank, J. 2006, *ApJ*, 643, 381
- Eggleton, P. P. 1983, *ApJ*, 268, 368
- Farmer, A. J. & Phinney, E. S. 2003, *MNRAS*, 346, 1197
- Fink, M., Hillebrandt, W., & Röpke, F. K. 2007, *A&A*, 476, 1133
- Fink, M., Röpke, F. K., Hillebrandt, W., Seitenzahl, I. R., Sim, S. A., & Kromer, M. 2010, *A&A*, 514, A53
- Frank, J., King, A., & Raine, D. J. 2002, *Accretion Power in Astrophysics: Third Edition*, ed. Frank, J., King, A., & Raine, D. J.
- Fryer, C. L. & Diehl, S. 2008, in *Astronomical Society of the Pacific Conference Series*, Vol. 391, *Hydrogen-Deficient Stars*, ed. A. Werner & T. Rauch, 335
- Fryxell, B., Olson, K., Ricker, P., Timmes, F. X., Zingale, M., Lamb, D. Q., MacNeice, P., Rosner, R., Truran, J. W., & Tufo, H. 2000, *ApJS*, 131, 273
- Guerrero, J., García-Berro, E., & Isern, J. 2004, *A&A*, 413, 257
- Guillochon, J., Dan, M., Ramirez-Ruiz, E., & Rosswog, S. 2010, *ApJ*, 709, L64
- Han, Z., Podsiadlowski, P., Maxted, P. F. L., & Marsh, T. R. 2003, *MNRAS*, 341, 669
- Hicken, M., Garnavich, P. M., Prieto, J. L., Blondin, S., DePoy, D. L., Kirshner, R. P., & Parrent, J. 2007, *ApJ*, 669, L17
- Hix, W. R., Khokhlov, A. M., Wheeler, J. C., & Thielemann, F. 1998, *ApJ*, 503, 332
- Howell, D. A., Sullivan, M., Nugent, P. E., Ellis, R. S., Conley, A. J., Le Borgne, D., Carlberg, R. G., Guy, J., Balam, D., Basa, S., Fouchez, D., Hook, I. M., Hsiao, E. Y., Neill, J. D., Pain, R., Perrett, K. M., & Pritchett, C. J. 2006, *Nature*, 443, 308
- Iben, Jr., I. & Tutukov, A. V. 1984, *ApJS*, 54, 335
- , 1986, *ApJ*, 311, 753
- Lee, W. H. & Ramirez-Ruiz, E. 2007, *New Journal of Physics*, 9, 17
- Lorón-Aguilar, P., Isern, J., & García-Berro, E. 2009, *A&A*, 500, 1193
- Marsh, T. R., Nelemans, G., & Steeghs, D. 2004, *MNRAS*, 350, 113
- Monaghan, J. J. 2005, *Reports on Progress in Physics*, 68, 1703
- Monaghan, J. J. & Gingold, R. A. 1983, *Journal of Computational Physics*, 52, 374
- Morris, J. P. & Monaghan, J. J. 1997, *J. Comput. Phys.*, 136, 41
- Motl, P. M., Frank, J., Tohline, J. E., & D'Souza, M. C. R. 2007, *ApJ*, 670, 1314
- Motl, P. M., Tohline, J. E., & Frank, J. 2002, *ApJS*, 138, 121
- Napiwotzki, R. 2009, *Journal of Physics Conference Series*, 172, 012004
- Nelemans, G., Portegies Zwart, S. F., Verbunt, F., & Yungelson, L. R. 2001a, *A&A*, 368, 939
- Nelemans, G., Yungelson, L. R., Portegies Zwart, S. F., & Verbunt, F. 2001b, *A&A*, 365, 491
- New, K. C. B. & Tohline, J. E. 1997, *ApJ*, 490, 311
- Paczynski, B. 1967, *Acta Astronomica*, 17, 287
- , 1971, *ARA&A*, 9, 183
- Pakmor, R., Kromer, M., Röpke, F. K., Sim, S. A., Ruiter, A. J., & Hillebrandt, W. 2010, *Nature*, 463, 61
- Rasio, F. A. & Shapiro, S. L. 1992, *ApJ*, 401, 226
- , 1994, *ApJ*, 432, 242
- , 1995, *ApJ*, 438, 887
- Rosswog, S. 2005, *ApJ*, 634, 1202
- , 2007, *MNRAS*, 376, L48
- , 2009, *New Astronomy Reviews*, 53, 78
- Rosswog, S., Ramirez-Ruiz, E., Hix, W. R., & Dan, M. 2008, *Computer Physics Communications*, 179, 184
- Rosswog, S., Speith, R., & Wynn, G. A. 2004, *MNRAS*, 351, 1121
- Ruiter, A. J., Belczynski, K., Benacquista, M., Larson, S. L., & Williams, G. 2010, *ApJ*, 717, 1006
- Saio, H. & Jeffery, C. S. 2000, *MNRAS*, 313, 671
- Segretain, L., Chabrier, G., & Mochkovitch, R. 1997, *ApJ*, 481, 355
- Silverman, J. M., Ganeshalingam, M., Li, W., Filippenko, A. V., Miller, A. A., & Poznanski, D. 2011, *MNRAS*, 410, 585
- Solheim, J. 2010, *PASP*, 122, 1133
- Timmes, F. X. & Swesty, F. D. 2000, *ApJS*, 126, 501
- Webbink, R. F. 1984, *ApJ*, 277, 355
- Yoon, S., Podsiadlowski, P., & Rosswog, S. 2007, *MNRAS*, 380, 933
- Yuan, R. F., Akerlof, C., Miller, J., Quimby, R., Peters, C., Thorstensen, J., Baltay, C., Bauer, A., Rabinowitz, D., Scalzo, R., Rigaudier, G., Pecontal, E., Buton, C., Copin, Y., Gangler, E., Smadja, G., Tao, C., Antilogus, P., Bailey, S., Pain, R., Pereira, R., Wu, C., Aldering, G., Aragon, C., Bongard, S., Childress, M., Loken, S., Nugent, P., Perlmutter, S., Runge, K., Thomas, R. C., Weaver, B. A., Birchall, D., Cough, J., Holtzman, J., Rau, A., Kasliwal, M., & Gal-Yam, A. 2007, *The Astronomer's Telegram*, 1212, 1